PHYSICAL REVIEW D **84,** 122002 (2011)

Measuring gravitomagnetic effects by a multi-ring-laser gyroscope

F. Bosi,[a] G. Cella,[b] and A. Di Virgilio[c]
INFN Sezione di Pisa, Pisa, Italy

A. Ortolan[d]
Laboratori Nazionali di Legnaro, INFN Legnaro (Padova), Italy

A. Porzio[e] and S. Solimeno[f]
University of Naples and CNR-SPIN, Naples, Italy

M. Cerdonio[g] and J. P. Zendri[h]
INFN Sezione di Padova, Padova, Italy

M. Allegrini,[i] J. Belfi,[j] N. Beverini,[k] B. Bouhadef,[l] G. Carelli,[m] I. Ferrante,[n]
E. Maccioni,[o] R. Passaquieti,[p] and F. Stefani[q]
University of Pisa and CNISM, Pisa, Italy

M. L. Ruggiero[r] and A. Tartaglia[s]
Politecnico of Torino and INFN, Torino, Italy

K. U. Schreiber[t] and A. Gebauer[u]
Technische Universitaet Muenchen, Forschungseinrichtung Satellitengeodaesie, Fundamentalstation Wettzell, 93444 Bad Kötzting, Germany

J-P. R. Wells[v]
Department of Physics and Astronomy, University of Canterbury, Christchurch 8020, New Zealand
(Received 26 July 2011; published 9 December 2011)

We propose an underground experiment to detect the general relativistic effects due to the curvature of space-time around the Earth (de Sitter effect) and to the rotation of the planet (dragging of the inertial frames or Lense-Thirring effect). It is based on the comparison between the IERS value of the Earth rotation vector and corresponding measurements obtained by a triaxial laser detector of rotation. The proposed detector consists of six large ring lasers arranged along three orthogonal axes. In about two years of data taking, the 1% sensitivity required for the measurement of the Lense-Thirring drag can be reached with square rings of 6 m side, assuming a shot noise limited sensitivity (20 prad/s/$\sqrt{\text{Hz}}$). The multigyros system, composed of rings whose planes are perpendicular to one or the other of three orthogonal axes, can be built in several ways. Here, we consider cubic and octahedral structures. It is shown that the symmetries of the proposed configurations provide mathematical relations that can be used to ensure the long term stability of the apparatus.

DOI: 10.1103/PhysRevD.84.122002 PACS numbers: 42.15.Dp, 42.30.Sy, 42.55.Lt, 91.10.Nj

[a]bosi@pi.infn.it
[b]giancarlo.cella@pi.infn.it
[c]angela.divirgilio@pi.infn.it
[d]antonello.ortolan@lnl.infn.it
[e]alberto.porzio@na.infn.it
[f]solimeno@na.infn.it
[g]cerdonio@pd.infn.it
[h]zendri@lnl.infn.it
[i]maria.allegrini@df.unipi.it
[j]belfi@df.unipi.it
[k]beverini@df.unipi.it
[l]bouhadef@df.unipi.it
[m]carelli@df.unipi.it
[n]isodoro.ferrante@pi.infn.it
[p]roberto.passaquieti@pi.infn.it
[q]fabio.stefani@df.unipi.it
[r]matteo.ruggiero@polito.it
[s]angelo.tartaglia@polito.it
[t]schreiber@fs.wettzell.de
[u]gebauer@fs.wettzell.de
[v]jon-paul.wells@canterbury.ac.nz

I. INTRODUCTION

The general theory of relativity is the most satisfactory description of gravitational phenomena. The theoretical breakthrough came with Einstein's geometrical representation of gravity: as different test masses fall in the same way in a gravitational field, gravity must be a property of space and time rather than of the masses themselves.

Until now, almost all successful tests of general relativity (Shapiro time delay [1], light deflection by the sun [2], perihelion shift of the orbit of Mercury [3]) have been probing the gravitational field of the Sun, without considering its proper rotation. However, general relativity predicts that the stationary field of a rotating body is different from the static field produced by the same nonrotating mass. The difference is known as gravitomagnetism (GM) and consists of a drag of space-time due to the mass currents. The rotational frame-dragging effect is also known as the Lense-Thirring (LT) [4] effect.

A direct experimental evidence of the existence of the GM field has been obtained so far by Ciufolini [5] and by Francis Everitt and the GP-B group [6]. The Lense-Thirring effect, averaged over several orbits, has been recently verified by analyzing the node orbital motion of two laser ranged freely falling satellites (LAGEOS-1 and LAGEOS-2) which orbit the Earth. In the measurement presented in Ref. [5], the two LAGEOS satellites were used to confirm the LT effect with an accuracy of the order of 10%. However, the launch of a third properly designed satellite, LARES, will give the opportunity to measure the LT effect with an accuracy of the order of 1% [7].

The possibility to detect Lense-Thirring with ring lasers has been discussed in the past [8,9]. Recently, it has been already pointed out that a multigyros system is able to test locally the Lense-Thirring effect [10]: an array of six, 6 m side, square ring lasers have enough sensitivity for this purpose. The rings must have different orientation in space. In the present paper we concentrate the attention on the symmetries of the rings arranged on the faces of a cube or along the edges of an octahedron, extracting the relevant relations important for the diagnostics of the system. At the end, we summarize and sketch the proposed experiment. For completeness we must mention that an experiment of the type we are planning and preparing could also be made, in principle, using matter waves instead of light. This possibility has been proved experimentally for various types of particles such as electrons [11], neutrons [12], Cooper pairs [13], calcium atoms [14], superfluid He3 [15], and superfluid He4 [16]. Cold atoms interferometry, in particular, yields very high sensitivity and it is suitable for space experiments because of the apparatus small size. However, atoms interferometry experiments in space do not provide an independent measurement of the Earth angular velocity, are affected by the mass distribution of the Earth, and test the average of the relativistic effect rather than the local one. Eventually, the comparison between in-space and on-ground measurements could be very valuable.

II. DETECTION OF GRAVITOMAGNETIC EFFECTS

Gravitomagnetism (GM) is a general relativistic phenomenon related to the presence of mass currents in the reference frame of a given observer. In the case of celestial bodies, including the Earth, and excluding translational motion with respect to the center of the body, gravitomagnetic effects are due to the absolute rotation of the massive source with respect to distant stars. When the Einstein equations in vacuum are applied to this kind of symmetry and are linearized (weak field approximation), GM is accounted for by the analogue of a magnetic field of a rotating spherical charge. In practice at the lowest approximation level, a dipolar GM field is obtained, with the dimensions of an angular velocity. Its explicit form in a nonrotating reference frame centered on the source (in our case the Earth center) is (see e.g. [17])

$$\boldsymbol{B} = \frac{2G}{c^2R^3}[\boldsymbol{J}_\oplus - 3(\boldsymbol{J}_\oplus \cdot \boldsymbol{u}_r)\boldsymbol{u}_r], \tag{1}$$

where $\boldsymbol{R} \equiv R\boldsymbol{u}_r$ is the position of the laboratory with respect to the center of the Earth and $\boldsymbol{J}_\oplus$ is the angular momentum of the Earth, whose modulus is of course given by the product of the moment of inertia of the planet multiplied by its angular velocity.

The effect produced by a field like (1) on a massive test body moving with velocity $\boldsymbol{v}$ looks like the one produced by a magnetic field on a moving charge: in fact, the geodesic equation in weak field approximation reads

$$\frac{d\boldsymbol{v}}{dt} = \boldsymbol{G} + \boldsymbol{v} \wedge \boldsymbol{B}, \tag{2}$$

where $\boldsymbol{G} = -GM/R^2\boldsymbol{u}_r$ is the Newtonian gravitational field, so that the effect can be described in terms of a gravitoelectromagnetic Lorentz force, where the Newtonian gravitational field plays the role of the gravitoelectric field (GE).

Furthermore, the rotation of the source of the gravitational field affects a gyroscope orbiting around it, in such a way that it undergoes the so-called Lense-Thirring precession, or dragging of the inertial frames of which the gyroscope defines an axis [17,18]. This phenomenon shows up also when one considers a freely falling body with local zero angular momentum: it will be seen as rotating by a distant observer at rest with the fixed stars [19].

A. Mechanical gyroscopes

Gravitomagnetic effects can in principle be measured applying different methodologies. The one that has most often been considered is focused on the behavior of a gyroscope, that can be either in free fall (on board an orbiting satellite) or attached to the rotating Earth. The

axis of the gyroscope is affected in various ways by the presence of a gravitational field. As for GM, a little mechanical gyroscope is the analogous of a small dipolar magnet (a current loop), so that it behaves as magnetic dipoles do when immersed in an external magnetic field.

When studying the motion around the Earth of a gyroscope whose spin vector is $\boldsymbol{S}$, one is led to the formula [3,17]

$$\frac{d\boldsymbol{S}}{dt} = \boldsymbol{\Omega}' \wedge \boldsymbol{S}. \tag{3}$$

In Appendix A we work out the explicit expression of $\boldsymbol{\Omega}'$ in general relativity and, more in general, in metric theories of gravity, using the parametrized post-Newtonian (PPN) formalism [20]: we show that it is related to the gravitomagnetic components g_{0i} of the metric tensor and its expression is given by [see Eqs. (A6)–(A10)] $\boldsymbol{\Omega}' = \boldsymbol{\Omega}_G + \boldsymbol{\Omega}_B + \boldsymbol{\Omega}_W + \boldsymbol{\Omega}_T$, so that we can distinguish four contributions, namely, the geodetic term $\boldsymbol{\Omega}_G$, the Lense-Thirring term $\boldsymbol{\Omega}_B$, the preferred frame term $\boldsymbol{\Omega}_W$, and the Thomas term $\boldsymbol{\Omega}_T$. All terms in $\boldsymbol{\Omega}'$ are called relativistic precessions, but properly speaking only the second is due to the intrinsic gravitomagnetic field of the Earth, namely, it is $\boldsymbol{\Omega}_B = -\frac{1}{2}\boldsymbol{B}$, and manifests the Lense-Thirring drag.

Ciufolini [21] deduced the relativistic precession of the whole orbital momentum of two LAGEOS satellites whose plane of the orbit is dragged along by the rotating Earth. Again on Eq. (3) was based the GP-B experiment, whose core was four freely falling spherical gyroscopes carried by a satellite in polar orbit around the Earth [6]. While time goes on and the available data grow it is expected that the Lense-Thirring drag will emerge from the behavior of the unique (so far) double pulsar system [22].

B. Using light as a probe

A different experimental approach consists in using light as a probe. In this case the main remark is that the propagation of light in the gravitational field of a rotating body is not symmetric. The coordinated time duration for a given space trajectory in the same sense as the rotation of the central source is different from the one obtained when moving in the opposite direction. This asymmetry would, for instance, be visible in the Shapiro time delay of electromagnetic signals passing by the Sun (or Jupiter) on opposite sides of the rotation axis of the star (or the planet) [23,24].

This property of the propagation of light is the one which we wish to exploit in our Earth-bound experiment using a set of ring lasers. In a terrestrial laboratory, light circulating inside a laser cavity in opposite directions is forced, using mirrors, to move along a closed path in space. What is closed from the view point of the laboratory is not so for a fixed-stars-bound observer, but the essential is that the two directions are not equivalent and that the two times required for light to come back to the active region are (slightly) different. As it happened already in the case of the mechanical gyroscopes, here too the difference in the two times of flight is made up of various contributions depending on the rotation of the axes of the local reference frame with respect to distant stars, on the fact that the local gravitational (Newtonian) potential is not null, and of course on the GM drag (which is our main interest). What matters, however, is that the final proper time difference (a scalar quantity) is invariant: it does not depend on the choice of the reference frame or of the coordinates.

Performing the calculation in linear approximation for an instrument with its normal contained in the local meridian plane (see the Appendix A details) we find

$$c\delta\tau = \frac{4A}{c}\Omega_\oplus\Big[\cos(\theta+\alpha) - 2\frac{GM}{c^2R}\sin\theta\sin\alpha + \frac{GI_\oplus}{c^2R^3}(2\cos\theta\cos\alpha + \sin\theta\sin\alpha)\Big], \tag{4}$$

where A is the area encircled by the light beams, α is the angle between the local radial direction and the normal to the plane of the instrument, measured in the meridian plane, and θ is the colatitude of the laboratory; $\Omega_\oplus$ is the rotation rate of the Earth as measured in the local reference frame (which includes the local gravitational time delay).

Equation (4) can also be written in terms of the flux of an effective angular velocity $\boldsymbol{\Omega}$ through the cross section of the apparatus:

$$\delta\tau = \frac{4}{c^2}\mathbf{A}\cdot\boldsymbol{\Omega}, \tag{5}$$

where $\mathbf{A} = A\boldsymbol{u}_n$ is the area enclosed by the beams and oriented according to its normal vector $\boldsymbol{u}_n$. In particular, it is $\boldsymbol{\Omega} = \boldsymbol{\Omega}_\oplus + \boldsymbol{\Omega}'$, and the term proportional to $\boldsymbol{\Omega}_\oplus$ is the purely kinematic Sagnac term, due to the rotation of the Earth, while $\boldsymbol{\Omega}' = \boldsymbol{\Omega}_G + \boldsymbol{\Omega}_B + \boldsymbol{\Omega}_W + \boldsymbol{\Omega}_T$ encodes the relativistic effects (see Appendix A).

For a ring laser in an Earth-bound laboratory, the geodetic and Lense-Thirring terms are both of order $\sim 10^{-9}$ with respect to the Sagnac term, while the Thomas term is 3 orders of magnitude smaller. As for the preferred frame term, the best estimates [25,26] show that this effect is about 2 orders of magnitude smaller than the geodetic and Lense-Thirring terms. Consequently, to leading order, the relativistic contribution to the rotation measured by the ring laser turns out to be $\boldsymbol{\Omega}' \simeq \boldsymbol{\Omega}_G + \boldsymbol{\Omega}_B$, which we aimed at measuring in our experiment. In other words, the goal of our experiment will be the estimate of $\boldsymbol{\Omega}'$ (see Fig. 1) which embodies the gravitomagnetic effects in a terrestrial laboratory.

In particular, the proposed experiment can also provide high precision tests of metric theories of gravity which are described in the framework of (PPN) formalism. In fact, from Eqs. (A22) and (A23), we see that, on setting for the rotating Earth $\boldsymbol{J} = I_\oplus\boldsymbol{\Omega}_\oplus$, we obtain

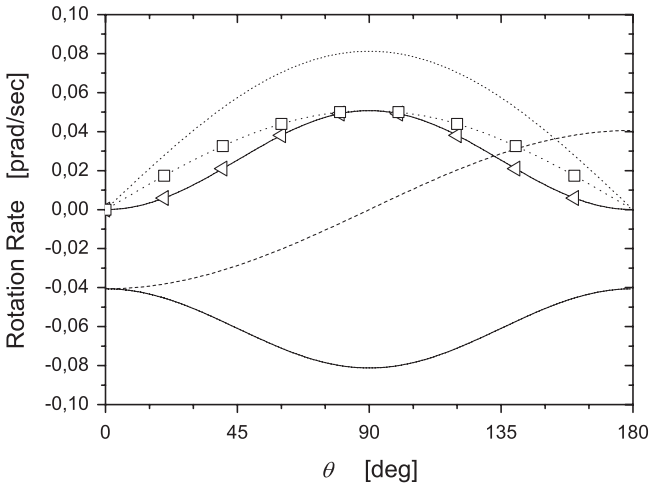

FIG. 1. The amplitude of the relativistic effects on the surface of the Earth, according to the theory of general relativity, in units of prad/s, as a function of the colatitude θ. The continuous, dashed, and dotted lines correspond to $\boldsymbol{\Omega}' = \boldsymbol{\Omega}_G + \boldsymbol{\Omega}_B$ projected along the directions: (i) parallel to $\boldsymbol{\Omega}_\oplus$ (i.e. $\Omega'_\parallel$); (ii) $\boldsymbol{u}_r$ (local radial or zenithal direction); and (iii) $\boldsymbol{u}_\theta$ (local North-South direction), respectively. To evaluate the contribution to $\boldsymbol{\Omega}'$ from $\boldsymbol{\Omega}_G$, we have projected $\boldsymbol{\Omega}_G$ along $\boldsymbol{\Omega}_\oplus$ (continuous line plus triangles) and $\boldsymbol{u}_\theta$ (dotted lines plus squares). We note that the gravitoelectric term has only the $\boldsymbol{u}_\theta$ component and therefore along the radial direction we have a pure gravito-magnetic term.

$$\boldsymbol{\Omega}_G = -(1+\gamma)\frac{GM}{c^2 R}\sin\vartheta\Omega_\oplus \boldsymbol{u}_\vartheta, \tag{6}$$

$$\boldsymbol{\Omega}_B = -\frac{1+\gamma+\frac{\alpha_1}{4}}{2}\frac{GI_\oplus}{c^2R^3}[\boldsymbol{\Omega}_\oplus - 3(\boldsymbol{\Omega}_\oplus\cdot\boldsymbol{u}_r)\boldsymbol{u}_r], \tag{7}$$

where α_1 and γ are PPN parameters (e.g. $\alpha_1 = 0$ and $\gamma = 1$ in general relativity) which account for the effect of preferred reference frame and the amount of space curvature produced by a unit rest mass, respectively.

As shown in Sec. VII B, from a high precision measurement of the vector $\boldsymbol{\Omega}'$ in the meridian plane, we should be able to place new constraints on the PPN parameters α_1 and γ.

III. THEORY OF THE MEASUREMENT: COMBINING TOGETHER THE RESPONSE OF SEVERAL RINGS

A. The response of a ring laser

A ring laser converts time differences into frequency differences. In fact, since the emission is continuous, the right-handed beam adjusts itself to give a standing wave whose wavelength is an integer submultiple of the space length of the loop P: $c\tau_+ = P = N\lambda_+$. The same happens with the left-handed beam, but being the total time different, also the wavelength of the corresponding standing wave will be different: $c\tau_- = N\lambda_-$. The two modes of the ring can have different N, a situation usually called "split mode," but the higher accuracy of the measurement has been obtained so far with the two modes with equal N. Considering the time of flight difference in terms of the wavelengths of the two standing waves, we see that

$$c\delta\tau = N(\lambda_+ - \lambda_-) = Nc\frac{f_- - f_+}{f^2} = P\lambda\frac{\delta f}{c}. \tag{8}$$

The ring-laser equation [27] relates the frequency splitting δf of the two optical beams inside the ring interferometer with the experienced rotation rate of its mirrors,

$$\delta f = \frac{4A}{\lambda P}\mathbf{u}_n\cdot\boldsymbol{\Omega}, \tag{9}$$

where P is the perimeter and λ is the laser wavelength. The response R of a ring laser to the rotation rate $\boldsymbol{\Omega}$, in units of rad/ sec, is simply a rescaling of the frequency splitting by the scale factor $S \equiv \frac{4A}{\lambda P}$, i.e.,

$$R \equiv \delta f/S = \mathbf{u}_n\cdot\boldsymbol{\Omega}. \tag{10}$$

The scale factor S plays a crucial role in the accuracy of the measurement of $\boldsymbol{\Omega}$ and to estimate the relativistic effects the ratio $\frac{4A}{\lambda P}$ must be known and kept at 10^{-10} accuracy level for months. The requirements to keep the apparatus in the optimal working conditions will be discussed in Sec. IV.

Since the effective angular velocity as well as the gravitomagnetic one is of the order of $10^{-9}\Omega_\oplus$, angles between vectors must be measured at the corresponding accuracy level. Unfortunately, the absolute measurement of $\boldsymbol{u}_n$ in the fixed stars reference system with the accuracy of nanoradians can hardly be achieved. However, we can relax this requirement by using $M \geq 3$ ring lasers oriented along directions $\boldsymbol{u}^\alpha$ ($\alpha = 1\ldots M$), where not all $\boldsymbol{u}^\alpha$ lie in the same plane. In fact, $\boldsymbol{\Omega}$ can be completely measured by means of its projections on at least three independent directions (e.g., defining a tridimensional Cartesian system) and the redundancies of the measurement can be used as a monitor and control of the stability of the directions $\boldsymbol{u}^\alpha$. We further assume that ring lasers have identical sensitivity and noise parameters. From an experimental point of view, this can be easily satisfied by building the devices with scale factors that differ less than %.

In order to simplify the sensitivity calculations of the system, one can consider multiaxial configurations endowed with symmetries. As all the ring-laser normals $\boldsymbol{u}^\alpha$ are equivalent in space, symmetric configurations should be more efficient in the rejection of spurious effects and in the control and monitoring of the relative orientation of the ring lasers. The natural choice is to take advantage of space symmetries of regular polyhedra, setting one ring for each plane parallel to their faces. If we do not consider the degeneration between opposite faces, we have $M = 3$ in the case of the cube, four for tetrahedron and octahedron, six for dodecahedron, and ten for icosahedron. There is

a peculiar geometry with $M = 3$, obtained by arranging the rings along the edges of an octahedron, where the different rings can be nested together, sharing 2 by 2 the same mirrors. We will refer to it in the following by speaking of ''octahedral configuration.'' The $M = 3$ is the minimum number of rings necessary to reconstruct the rotational vector, but a redundancy is very appropriate to enhance statistics and to have control tests on the geometric accuracy.

In general, by simple arguments, one can demonstrate that, for regular polyhedra configuration,

$$\sum_{\alpha=1}^{M} \boldsymbol{u}_\alpha = \mathbf{0} \qquad (M > 3) \tag{11}$$

and that

$$\sum_{\alpha=1}^{M} (\boldsymbol{\Omega} \cdot \boldsymbol{u}_\alpha)^2 = \frac{M}{3} |\boldsymbol{\Omega}|^2 \qquad (M \geq 3). \tag{12}$$

As a consequence, one can study linear and quadratic combinations of ring-lasers responses R_α which are invariant under permutations of the ring laser labels α, i.e. $L = \sum_\alpha R_\alpha$ and $Q = \sum_\alpha R_\alpha^2$. For nonsymmetric configurations we can generalize their definition as $L = \sum_\alpha L_\alpha R_\alpha$ and $Q = \sum_\alpha Q_{\alpha\beta} R_\alpha R_\beta$, where L_α and $Q_{\alpha\beta}$ are suitable constants which depend on $\boldsymbol{u}_\alpha$. The interest in such linear or quadratic forms relies on their behaviors in the presence of noise fluctuations or variations of the geometry of the configuration.

They also allow us to carry out analytical estimates of the overall sensitivity of a triaxial system of ring laser to relativistic effective rotation rates.

B. Requirements for the geometry of the configuration

The response of each ring laser can be conveniently written as

$$R_\alpha = \boldsymbol{\Omega} \cdot (\boldsymbol{u}_\alpha + \delta \boldsymbol{u}_\alpha) + \varepsilon_\alpha, \tag{13}$$

where $\delta \boldsymbol{u}_\alpha \equiv \delta S_\alpha \boldsymbol{u}_\alpha + \delta \boldsymbol{\vartheta}_\alpha \wedge \boldsymbol{u}_\alpha$ account for systematic errors in the scale factors and orientations in space and ε_α represents the additive noise that affects the rotation measurement R_α, that we assume averaged on the observation time $T \simeq 1$ day. We assume as well that ε_α are Gaussian distributed random variables with zero mean and variance σ_Ω^2. Modulus $|\delta \boldsymbol{u}_\alpha| \simeq \delta S_\alpha$ and direction $\delta \boldsymbol{\vartheta}_\alpha \wedge \boldsymbol{u}_\alpha$ represent the deviations from regular polygon geometry in the plane and from polyhedra geometry in the space, due to scale factor fluctuations δS_α and infinitesimal rotations $\delta \boldsymbol{\vartheta}_\alpha$, respectively. In what follows the crucial assumption is that systematic errors (scale factors and relative alignment of $\boldsymbol{u}_\alpha$) are negligible with respect to statistical errors, i.e. $|\boldsymbol{\Omega} \cdot \delta \boldsymbol{u}_\alpha| < \sigma_\Omega$ or equivalently $|\delta \boldsymbol{u}_\alpha| < \sigma_\Omega / \Omega$, while the dihedral angles $\arccos(\boldsymbol{u}_\alpha \cdot \boldsymbol{u}_\beta)$ can nearly approximate a regular polyhedron configuration.

Redundancy of responses, if $M > 3$ rings are involved, can be used to control systematic errors projected along the direction of $\boldsymbol{\Omega}$. In fact, the rigidity of the configuration imposes some linear kinematic constraints among different estimates of the laboratory rotation. In general, any linear combination of three responses R_α gives an estimate of the local rotation $\boldsymbol{\Omega}$ and we can test the consistency among different estimates by means of the ordinary least square fit. A very simple linear constraint can be found for regular polyhedral configurations

$$L = \sum_{\alpha=1}^{M} R_\alpha \tag{14}$$

and we will illustrate its statistical property as an example of the power of the method.

From the definition of L immediately follows that it is Gaussian distributed with zero mean and standard deviation $\sigma_L = \sqrt{M} \sigma_\Omega$. In addition, possible misalignments $\delta \boldsymbol{\vartheta}_\alpha \wedge \boldsymbol{u}_\alpha$ or scale factor fluctuations $\delta S_\alpha \boldsymbol{u}_\alpha$ are amplified by a factor of Ω in the mean value of L:

$$\langle L \rangle = \sum_{\alpha=1}^{M} \boldsymbol{\Omega} \cdot \delta \boldsymbol{u}_\alpha \tag{15}$$

$$= \Omega \sum_{\alpha=1}^{M} (\delta S_\alpha \boldsymbol{u}_\alpha + \delta \boldsymbol{\vartheta}_\alpha \wedge \boldsymbol{u}_\alpha)^{\parallel}, \tag{16}$$

without affecting the corresponding variance σ_L^2. Thus, $\langle L \rangle$ can be used as a ''null constraint'' which is minimum when the configuration geometry is a regular polyhedron, and so the overall mean error parallel to $\boldsymbol{\Omega}$ can be monitored at $\sim \sqrt{M} \sigma_\Omega / \Omega \simeq 10^{-10}$ accuracy level.

C. Estimate of the parallel component of the relativistic effective rotation vector

An estimate of Ω^2 for symmetric configurations readily follows from Eq. (12):

$$Q = \frac{3}{M} \sum_{\alpha=1}^{M} R_\alpha^2 \tag{17}$$

$$= \Omega^2 + \frac{6}{M} \sum_{\alpha=1}^{M} \varepsilon_\alpha \boldsymbol{\Omega} \cdot \boldsymbol{u}^\alpha + \frac{3}{M} \sum_{\alpha=1}^{M} \varepsilon_\alpha^2. \tag{18}$$

Its mean value and standard deviation read (see Appendix B)

$$\langle Q \rangle = \Omega^2 + \tfrac{1}{3} \sigma_\Omega^2 \tag{19}$$

$$\sigma_Q = \sqrt{\frac{18}{M} \sigma_\Omega^4 + \frac{12}{M} \Omega^2 \sigma_\Omega^2}. \tag{20}$$

In addition, one can demonstrate that Q is noncentral χ^2 distributed with M degrees of freedom and noncentrality

parameter Ω^2. In order to estimate the relativistic effective rotation, we must subtract $\Omega_\oplus$ from the rotation rate estimated in the laboratory. To this end we calculate the difference $\Delta \equiv (Q - \Omega_\oplus^2)$ that, in the limit of high signal to noise ratio (SNR) ($|\Omega|/\sigma_\Omega \gg 1$), tends to be Gaussian distributed with mean

$$\langle \Delta \rangle \simeq 2\Omega_\oplus \Omega'_\parallel \tag{21}$$

and standard deviation

$$\sigma_\Delta \simeq (2\sqrt{3}/\sqrt{M})\Omega_\oplus \sigma_\Omega, \tag{22}$$

where we have neglected terms of the order of σ_Ω/Ω. The SNR $= \langle \Delta \rangle/\sigma_\Delta$ of the parallel component of relativistic effective rotation is increased by a factor of $\sqrt{M/3}$ with respect to the sensitivity of each ring laser.

The advantage of this approach is that we compare scalar quantities (moduli of rotation vectors) measured with respect to the local and distant stars reference systems. Its drawback is the very poor sensitivity to the perpendicular component $\Omega_\perp$ of the relativistic effective rotation. In fact, $\Omega^2 - \Omega_\oplus^2 = 2\boldsymbol{\Omega}' \cdot \boldsymbol{\Omega}_\oplus + |\boldsymbol{\Omega}'|^2$, and the ratio between the second term (which is associated to the perpendicular component as $|\boldsymbol{\Omega}'|^2 = \Omega_\parallel'^2 + \Omega_\perp'^2$) and the first term is $\sim GM/c^2R \simeq 10^{-10}$.

It is worth noticing that statistical fluctuations of L (control of geometry by redundancy) and Q (measure of relativistic effects) are uncorrelated, and that they tend to be independent in the limit of high SNR.

D. Estimate of the components of the relativistic effective rotation vector

By arranging the response of ring lasers R_α as M-tuples in a M-dimension vector space $\boldsymbol{R} = (R_1, R_2, R_3, \ldots, R_M)$, we can easily define projection operators that allow the estimate of local meridian plane $\mathcal{M}$ and also the direction $\boldsymbol{w}$ of $\boldsymbol{\Omega}$ in the physical space. Moreover, the norm of projected random vectors are described by remarkably simple statistics. According to the definition of the matrix product we have $\boldsymbol{R} = \boldsymbol{N\Omega} + \boldsymbol{\varepsilon}$, where $\boldsymbol{N}$ is a $M \times 3$ matrix whose elements are $\boldsymbol{N}_{\alpha i} = (u_\alpha)_i$ and $\boldsymbol{\varepsilon} = (\varepsilon_1, \varepsilon_2, \varepsilon_3, \ldots, \varepsilon_M)$. Thus, the random vectors $\boldsymbol{R}$ can be projected on the linear subspaces $\mathcal{P}_\mathcal{M}$ and $\mathcal{Q}_\mathcal{M}$ of dimensions 2 and $M - 2$, which represent, respectively, a plane in the physical space and its complementary space. The physical symmetry of the rotating Earth imposes that the relativistic effective rotation vectors and $\boldsymbol{\Omega}_\oplus$ lie in the same plane, i.e. the meridian plane, and therefore the knowledge of the orientation of this plane is crucial if we want to measure not only the modulus but the whole vector. We recall that a plane is defined as the set of the points $s\boldsymbol{v} + t\boldsymbol{w}$, where s and t range over all real numbers, $\boldsymbol{v}$ and $\boldsymbol{w}$, are given orthogonal unit vectors in the plane.

The parallelism of $\boldsymbol{v} \wedge \boldsymbol{w}$ with the normal to the meridian plane can be tested under the hypothesis that the rotation signal is fully located in the $\mathcal{P}_\mathcal{M}$ subspace while the $\mathcal{Q}_\mathcal{M}$ subspace contains only noise. The test can be easily performed over the norms of the two projections $E_P(\boldsymbol{v}, \boldsymbol{w}) \equiv \|\boldsymbol{P}_{\boldsymbol{v},\boldsymbol{w}}\boldsymbol{R}\|^2$ and $E_Q(\boldsymbol{v}, \boldsymbol{w}) \equiv \|\boldsymbol{Q}_{\boldsymbol{v},\boldsymbol{w}}\boldsymbol{R}\|^2$, where we have introduced the symbol $\|\boldsymbol{R}\| = (\sum_{\alpha=1}^M R_\alpha^2)^{1/2}$ to indicate the L-2 norm in the M-dimensional Euclidean response space. The $M \times M$ projection matrices $\boldsymbol{P}_{\boldsymbol{v},\boldsymbol{w}}$ and $\boldsymbol{Q}_{\boldsymbol{v},\boldsymbol{w}}$ can be written explicitly as functions of the unit vectors $\boldsymbol{v}$ and $\boldsymbol{w}$

$$\boldsymbol{P}_{\boldsymbol{v},\boldsymbol{w}} = \boldsymbol{NV}(\boldsymbol{NV})^T \tag{23}$$

$$\boldsymbol{Q}_{\boldsymbol{v},\boldsymbol{w}} = \boldsymbol{I} - \boldsymbol{NV}(\boldsymbol{NV})^T, \tag{24}$$

where $\boldsymbol{V}$ is a 3×2 matrix with columns $\boldsymbol{v}$ and $\boldsymbol{w}$, and $\boldsymbol{I}$ is the $M \times M$ identity matrix. As shown in Appendix B, the probability distribution of E_P is noncentral χ^2 with 2 degrees of freedom and noncentrality parameter Ω^2, while E_Q should be χ^2 distributed with M-2 degrees of freedom.

The best estimate of $\boldsymbol{v}$ and $\boldsymbol{w}$ is then obtained by

$$(\hat{v}, \hat{w}) = \arg\max_{\boldsymbol{v},\boldsymbol{w}} \|\boldsymbol{P}_{\boldsymbol{v},\boldsymbol{w}}\boldsymbol{R}\|^2, \tag{25}$$

where the $\max_{\boldsymbol{u},\boldsymbol{w}}$ is taken over the unit sphere. The direction of the Earth rotation axis can be estimated as a particular case of Eq. (10). In fact, the projectors $\boldsymbol{P}_{\boldsymbol{w}}$ and $\boldsymbol{Q}_{\boldsymbol{w}}$ can be obtained by substituting the matrix $\boldsymbol{V}$ for the 3×1 matrix $\boldsymbol{W}$ with columns $\boldsymbol{w}$. The difference lies in the dimension of the corresponding subspaces, i.e., $\mathcal{P}_\mathcal{W}$ and $\mathcal{Q}_\mathcal{W}$ have dimension 1 and M-1, respectively. It is worth noticing that the maximum of Eq. (25) can be computed by an analytical formula both for the location of the meridian plane and the direction of the Earth rotation axis. In fact, if we introduce in the local reference frame the (local) spherical coordinate (R, Θ, and Φ) (we use capital letters to avoid confusion with Sec. II) and parametrize the unit vectors $\boldsymbol{v}$ and $\boldsymbol{w}$ with these angles, for instance $\boldsymbol{w} = (\cos\Phi\sin\Theta, \sin\Phi\sin\Theta, \cos\Theta)$ and $\boldsymbol{v} = (\cos\Phi\cos\Theta, \sin\Phi\cos\Theta, -\sin\Theta)$, we have that the maximum of $\|\boldsymbol{P}_{\boldsymbol{v},\boldsymbol{w}}\boldsymbol{R}\|^2$ and $\|\boldsymbol{P}_{\boldsymbol{w}}\boldsymbol{R}\|^2$ is achieved for

$$\tan\hat{\Theta} = \left(\frac{\boldsymbol{R}^T\boldsymbol{F}\boldsymbol{R}}{\boldsymbol{R}^T\boldsymbol{H}\boldsymbol{R}}\right)^{1/2} \qquad \tan\hat{\Phi} = \left(\frac{\boldsymbol{R}^T\boldsymbol{K}\boldsymbol{R}}{\boldsymbol{R}^T\boldsymbol{J}\boldsymbol{R}}\right)^{1/2}, \tag{26}$$

where $\boldsymbol{F}$, $\boldsymbol{H}$, $\boldsymbol{K}$, $\boldsymbol{J}$ are $M \times M$ symmetric matrices which are functions of the $\boldsymbol{u}_\alpha$ alone.

In general, there are no analytical calculations for mean and variance of $\hat{\boldsymbol{v}}$, $\hat{\boldsymbol{w}}$ and one must run Monte Carlo simulations to get their estimates. However, in the limit of high SNR E_P and E_Q tend to be Gaussian distributed, as well as fluctuations of $\hat{\boldsymbol{v}}$ and $\hat{\boldsymbol{w}}$ around their mean values. The same reasoning holds true also for the estimation of $\hat{\Theta}$ and $\hat{\Phi}$.

The validity of the proposed experimental configuration has been checked by a numerical simulation over a period

of one year of the six responses of the octahedral configuration oriented as in Fig. 23 of Sec. V C. In order to simplify the calculations we assume that the laboratory colatitude is $\theta = \pi/4$ and that the normal to the plane of a ring forms a $\pi/4$ angle with respect to the Earth axis, and another normal is orthogonal to the former and forms again a $\pi/4$ angle with the west-east direction. This configuration is close to a possible experimental arrangement at the Gran Sasso National Laboratories (LNGS) within a few degrees. The directions of the unit vector $\boldsymbol{u}_\alpha$ in the local reference frame are

$$\begin{aligned} \boldsymbol{u}_1 &= \boldsymbol{u}_4 = \left(\frac{1}{2}, \frac{1}{\sqrt{2}}, \frac{1}{2}\right) \\ \boldsymbol{u}_2 &= \boldsymbol{u}_5 = \left(-\frac{1}{2}, \frac{1}{\sqrt{2}}, -\frac{1}{2}\right) \\ \boldsymbol{u}_3 &= \boldsymbol{u}_6 = \left(-\frac{1}{\sqrt{2}}, 0, \frac{1}{\sqrt{2}}\right) \end{aligned} \tag{27}$$

and the rotation signal for the six rings are equal within a factor $\sqrt{2}$. We assume one mean sidereal day $T_S = 86\,164.0989$ s of integration and a noise standard deviation $\sigma_\Omega = 7 \times 10^{-2}$ prad/s. The variance σ_Ω is extrapolated from present "G" sensitivity at 10^4 s and scaling by a factor 5, due by the increase of the ring size and the power of the laser of a factor 1.5 and 10, respectively. The relativistic rotation contributions $\Omega'_r = -2.8 \times 10^{-2}$ prad/s and $\Omega'_\theta = -5.6 \times 10^{-2}$ prad/s have been added to the Earth rotation vector $\boldsymbol{\Omega}_\oplus$, as estimated by IERS [28]. The component of relativistic effects parallel to $\boldsymbol{\Omega}_\oplus$ is $\Omega'_\parallel = (\Omega'_\theta + \Omega'_r)/\sqrt{2} = 5.9 \times 10^{-2}$ prad/s. Using Eq. (10) we calculated the responses of the six rings and then we injected the Gaussian noise. In Fig. 2 we show the histograms of $T_S\Delta/(2\pi)$ accumulated for 90 and 366 sidereal days. The corresponding mean values of the parallel component of relativistic effects are -6.0×10^{-2} prad/s and -6.2×10^{-2} prad/s with standard deviations 4.7×10^{-3} prad/s and 2.6×10^{-3} prad/s, respectively. Thus, a $\sim$10% accuracy can be achieved in three months by simply comparing the square modulus of rotation vectors. In order to give a full estimate of the vector $\boldsymbol{\Omega}'$, we have also explicitly calculated day by day the angles $\hat{\Theta}$ and $\hat{\Phi}$ for describing the orientation of the meridian plane and the direction of the Earth rotation vector. The results are summarized in Figs. 3 and 4, where we report the time evolution of these angles, and in Fig. 5, where we show the corresponding annual polar motion.

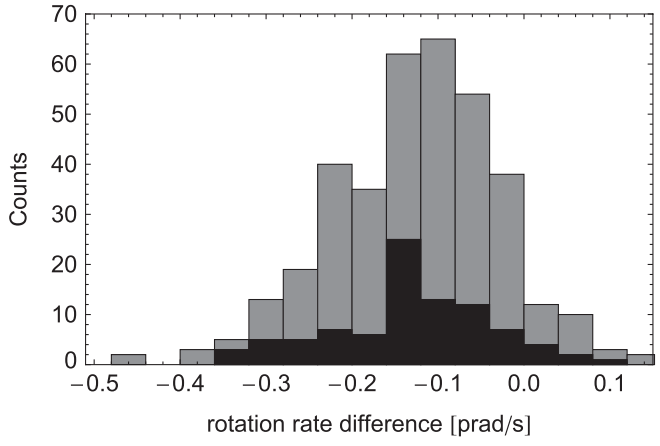

FIG. 2. Histograms of the difference Δ between Q and $\Omega^2_\oplus$, normalized with the mean sidereal day, collected for three months (dark histogram) and one year (light histogram).

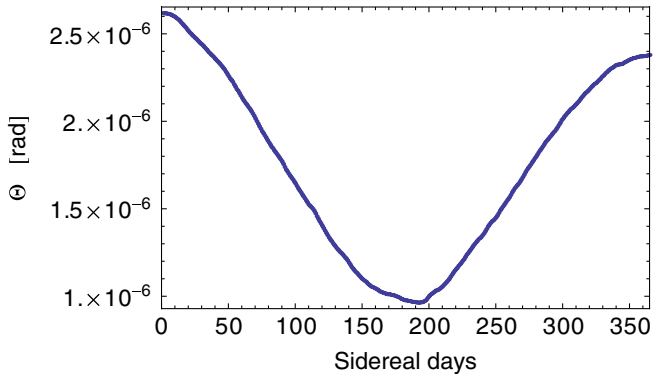

FIG. 3 (color online). Change of the angle Θ due to polar motion as measured by the ring-laser responses in one year.

By synchronizing the polar motion measured in the local reference system with the polar motion measured by IERS in the fixed star reference system, the two reference frames will coincide within the accuracy of the measurement of $\boldsymbol{\Omega}$ and $\boldsymbol{\Omega}_\oplus$, say one part of 10^{10}. As a final remark, we point out that the full measurement of the vector $\boldsymbol{\Omega}'$ allows for us the estimate of $\Omega'_\perp \simeq 2 \times 10^{-2}$ prad/s with a standard deviation of the same order of magnitude of the estimate of $\Omega'_\parallel$. This represents an increase of the relativistic

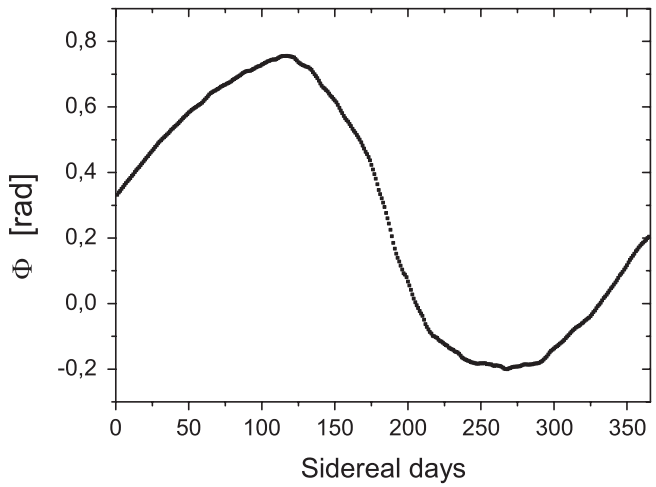

FIG. 4. Change of the angle Φ due to polar motion as measured by the ring-laser responses in one year. Note the large variation of Φ which corresponds to a nearly complete precession cycle of the Earth axis in one year.

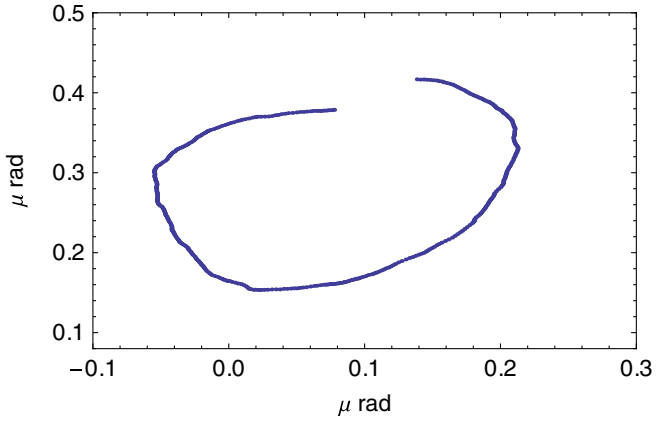

FIG. 5 (color online). The estimated polar motion from the six ring-laser responses.

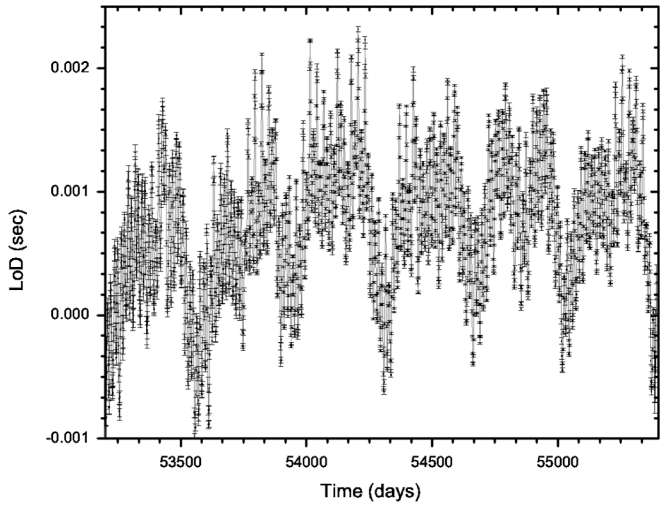

FIG. 6. The change of the length of the day (LoD) over the past six years from the IERS 05C04 time series. Notice that estimated errors of LoD decreased in the past years to a level which corresponds to 10^{-14} rad/ sec , i.e. 0.1 ppb $\Omega_\oplus$.

rotation signal of ~30%. However, the estimate of $\mathbf{\Omega}'$ is crucial to separate the geodetic from Lense-Thirring contributions and/or to measure the PPN parameters α_1 and γ.

E. The Earth motion and feasibility of the experiment

Since our goal is the estimate of the Lense-Thirring effect at few % accuracy, the independent measurement of $\mathbf{\Omega}_\oplus + \mathbf{\Omega}_{\rm REL}$, which represents the rotation of the laboratory with respect to distant stars, must be determined to $10^{-10}\Omega_\oplus$. Because of tidal forces and to the exchange of angular momentum between the solid Earth and geophysical fluids, the angular velocity of the Earth varies in time, both in direction and modulus. Changes in modulus correspond to a variation of the length of the day (LoD) of few milliseconds with respect to atomic clocks. The direction of the rotation axis of the Earth varies with respect to both the fixed stars and the Earth-fixed reference frames. Nowadays, the best Earth rotation monitoring is provided by the IERS 05C04 time series [28] which are routinely obtained using the geodetic space techniques VLBI (very long baseline interferometry), SLR (satellite laser ranging), GPS (global positioning system), and DORIS (Doppler orbitography and radiopositioning integrated by satellite).

In Figs. 6 and 7 we report the length of the day (LoD) and the pole position with the corresponding errors of the last six years. It is worth noticing that the achieved precision is 0.001 ms in the LoD and 0.1 μarcsec in the pole position.

Further improvements are expected in the next few years and the overall errors in LoD and pole position should decrease of a factor 10 that is crucial for a 1% measurement of the relativistic rotation terms. However, the IERS 05C04 time series is already sufficient to get $|\mathbf{\Omega}_\oplus|$ with 3% accuracy.

For what concerns the differential rotation of the laboratory with respect to the rotation estimated by IERS, it is expected to be sufficiently small to contribute to $\Omega_\oplus$ only through $\mathbf{\Omega}_{\oplus\|}$. However, $\mathbf{\Omega}_{\rm REL}$ is still largely unknown due to possible microrotations of the crust of the Earth. This is one of the causes limiting the performances of G in Wettzell: the Earth crust motion caused by atmospheric changes. It is assumed that an underground facility is less sensitive to this kind of noise sources. It is as well important to keep the experiment close to VLBI stations. The underground Gran Sasso Laboratories is placed halfway between two relatively close VLBI stations, Medicina [29] and Matera [30] which can provide estimates of the crustal motion of the Adriatic plate [31]. A significant contribution to $\mathbf{\Omega}_{\rm REL}$ comes from the "diurnal polar motion" (periodic motion of the Earth crust due to tides) and consists in periodic changes of amplitude $\sim 10^{-7}\Omega_\oplus$. This effect has

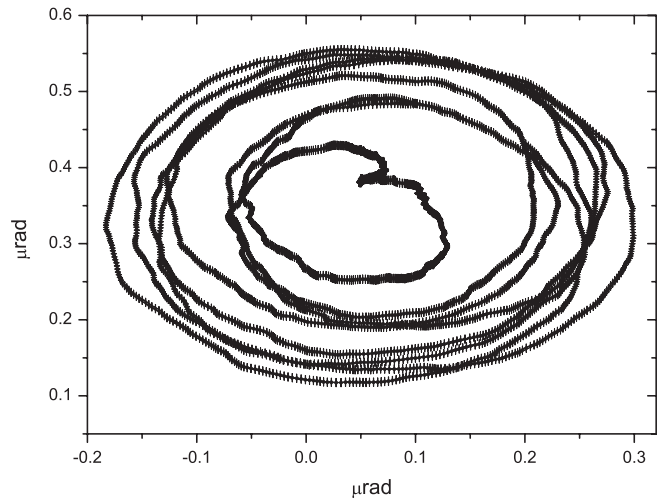

FIG. 7. The change of the direction of the Earth rotation axis (i.e. pole position) over the past six years from the IERS 05C04 time series. Estimated errors are also plotted.

been already measured by large ring-laser gyroscopes [32], and can be accurately modeled and then subtracted from ring-laser responses.

We conclude that by means of available geodesics and geophysics techniques, provided that the experiment is located in an area with very low relative angular motion (Ω_{REL}), a suitable triaxial detector of rotation can in principle detect Ω' with % precision.

IV. THE "REAL APPARATUS", THE PRESENT SENSITIVITY OF G IN WETTZELL

A. Sensor properties

A closer look at Eq. (9) reveals that there are three basic effects one has to carefully account for. These are:

(i) scale factor stability ($4A/\lambda P$)
(ii) orientation of the gyroscope with respect to the instantaneous axis of rotation of the Earth
(iii) instantaneous rate of rotation change of the Earth—Length of Day (LoD).

The scale factor for all practical purposes has to be held constant to much better than 1 part in 10^{10}. Otherwise the frame-dragging parameter cannot be determined unambiguously. For G, the base of the gyroscope has been manufactured from Zerodur, a glass ceramic with a thermal expansion coefficient of $\alpha < 5 \times 10^{-9}/^{\circ}\mathrm{C}$. Furthermore, the instrument is located in a thermally insulated and sealed environment with typical temperature variations of less than 5 mK per day. However, because the underground laboratory is only at a depth of 5 m, there is still a peak to peak temperature variation of about 1° per year, accounting for the change of seasons. Changes in the atmospheric pressure also affect the dimensions of the ring-laser structure by changing the compression of the Zerodur block and cannot be neglected. Hence, G is kept in a pressure stabilized enclosure. A feedback system based on the determination of the current value of the optical frequency of the lasing mode of one sense of propagation allows for active control of the pressure inside the steel vessel such that an overall geometric scale factor stability of better than 10^{-10} is routinely obtained. At the same time the design of the instrument is made as symmetric as possible. So changes in area and perimeter are compensated with a corresponding change in wavelength as long as no shear forces are present and the longitudinal mode index stays the same.

A typical eight day long measurement sequence of rotation rate data from the G ring laser is shown in Fig. 8. In order to demonstrate the obtained sensor sensitivity, we have subtracted the mean Earth rotation rate from the gyroscope data. The y axis gives the measured variation of the rate of rotation, while the x axis shows the time expressed in the form of the modified Julian date. Each data point was taken by integrating over 30 min of measurement data. There are several distinct signal contributions in the data, which come from known geophysical

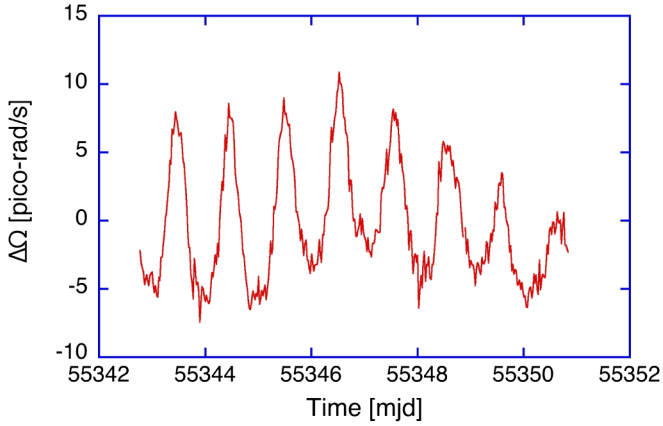

FIG. 8 (color online). Approximately eight days of raw G data taken with 30 minutes of integration time. One can clearly see the contributions from diurnal polar motion, solid Earth tides, and local tilt.

effects. The most prominent signal is caused by diurnal polar motion [33]. The polar motion data is superimposed by a tilt signal caused by the semidiurnal and diurnal tides of the solid Earth, distorting the otherwise sinusoidal diurnal frequencies slightly. At the Geodetic Observatory in Wettzell, the tilt effects of the solid Earth tides can be as large as 40 nrad in amplitude. In Fig. 8 the diurnal signal is dominated by the polar motion [34]. Less evident in Fig. 8 are the effects from local tilt, which contains periodic signals of tidal origin as well as nonperiodic signals. The latter are nonperiodic and usually change slowly over the run of several days. High resolution tiltmeters inside the pressure stabilizing vessel of the G ring laser keep track of these local effects and the data is corrected for gravitational attraction (atmosphere, sun and moon) [33]. Large nonperiodic local tilts occur most prominently after abundant rainfall, indicating hydrological interactions with the rock and soil beneath the ring-laser monument. Figure 9 shows the east component of three tiltmeters installed (i) on a gravimeter pillar at the surface, (ii) in 6 m depth, and (iii) in 30 m depth.

While the tiltmeter in 30 m depths clearly shows the periodic signal of the solid earth tides, the tilt record of the instruments near to the surface is dominated by large

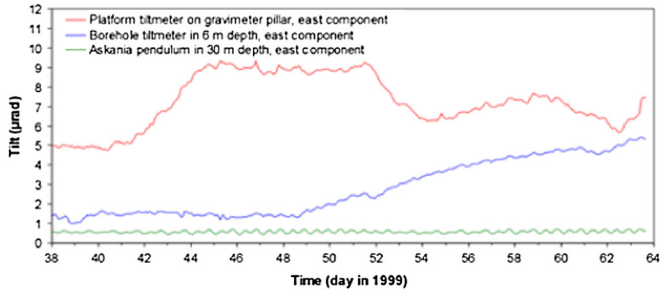

FIG. 9 (color online). Measurement of local tilts as a function of depth in the Earth.

nonperiodic signals hydrological, thermoelastic, and barometric origin. Several investigations have shown that the site and the installation depths of tiltmeters have a major impact on environmental noise mainly coming from hydrology [35–38] has shown that even in 100 m depths effects caused by hydrological changes are detectable, but strongly reduced in comparison to a 50 m deep installation. First investigations related to topographic and temperature induced effects were carried out by [39,40]. Detailed investigations using the finite-element method have shown that these effects can amount to more than 10 nrad [41,42]), while the distance between the source and the location of observation can be several hundred meters. Additionally, recent work using the G ring-laser data reveals that effects caused by wind friction at the Earth surface yields to high frequency rotations of large amplitudes.

The large seasonal temperature effect on the G ring laser as well as the substantial local tilt signals and the rather high ambient noise level of our near soil surface structures give reasonable hope of much better performances of a ring-laser installation in a deep underground laboratory such as the Gran Sasso Laboratories.

For the detection of fundamental physics signals, one has to remove all known perturbation signals of the Earth from the ring-laser time series. Furthermore, we have applied 2 h of averaging of the data in order to reduce the effect from short period perturbations. Figure 10 shows an example. In Fig. 11 we show the current sensitivity expressed in term of Allan deviation of the G, the expected sensitivity of each ring laser at Gran Sasso Laboratories, and the relevant geophysical signal.

In order to reduce the local orientation uncertainties, which remain after local tilts measured with the high resolution tiltmeters have been removed, averaging as indicated above was applied to a series of 30 days of data collection, including the period shown in Fig. 8. It can be expected that a similar data set from the Gran Sasso Laboratory would become substantially smoother, since most of the perturbations, caused by ambient atmosphere–topsoil interaction still contained in the data of Fig. 10 would no longer exist in the deep underground facility. Changing hydrologic conditions presumably causing small local rotation and temperature variations, atmospheric pressure, and wind loading are among the sources for the systematic signatures in the residual data.

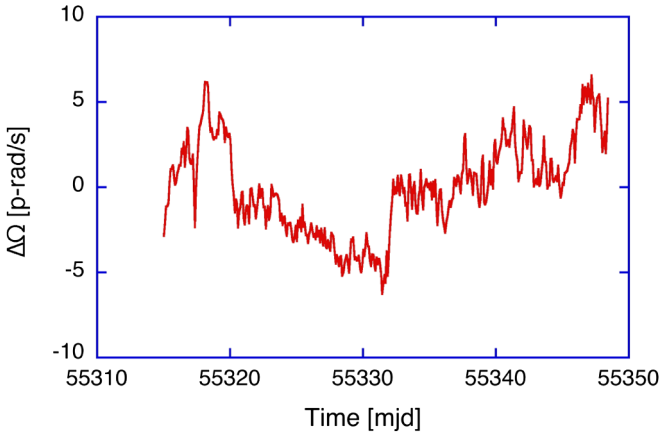

FIG. 10 (color online). The rotation rate of the Earth measured with the G ring laser as a function of time. Averaging over 2 h was applied to a corrected data set, where all known geophysical signals have been removed.

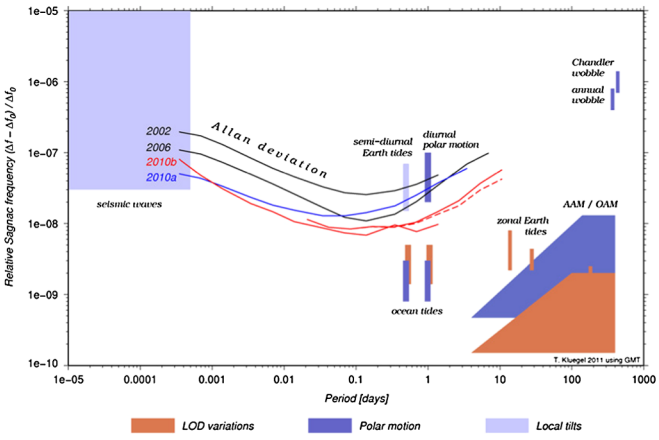

FIG. 11 (color online). Resolution and stability of G, compared with Earth signals.

V. CONFIGURATION OF A TRIAXIAL DETECTOR

From now on, we will restrict our analysis to 24 m perimeter rings, arranged in two configurations that are of some experimental interest, i.e. six ring lasers rigidly mounted on the faces of a cube, as shown in Fig. 12, and three ring lasers oriented along the edges of an octahedron, see Fig. 13. The cubic configuration requires 24 mirrors forming six independent rings and the extension of the

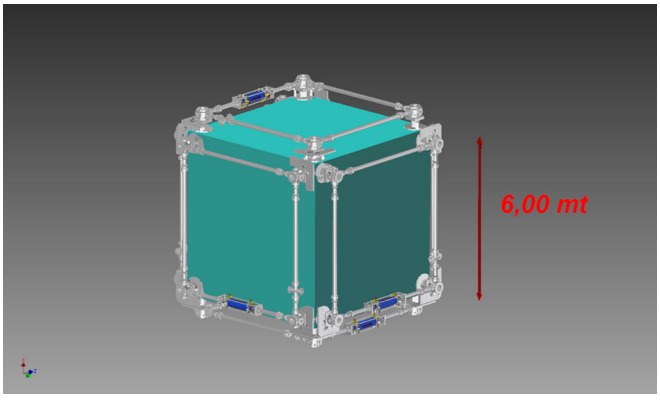

FIG. 12 (color online). Six rings arranged on the faces of a cube, using the GEOSENSOR design, which has been successfully used so far for middle size rings, as our prototype G-Pisa.

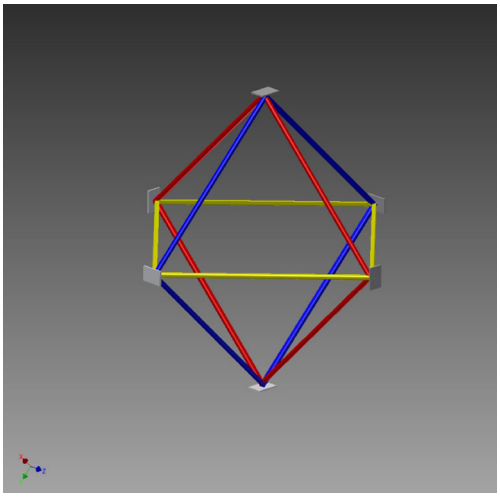

FIG. 13 (color online). Three rings are formed using six mirrors located on the vertices of an octahedron.

GEOSENSOR design is straightforward (see Sec. V C); while the octahedral configuration require six mirrors only to form three orthogonal rings. By itself the configuration which uses a cube is redundant, each ring has a parallel companion, which can be used for the study of systematics. For the octahedron configuration the implementation of the GEOSENSOR design needs further development. Redundancy can be easily obtained constructing a second octahedron with planes parallel to the other one. The two structures should be built very close to each other, in order to keep as much as possible the whole apparatus compact; in this way six rings are available, analogously to the cube configuration, see Fig. 14. This configuration has the advantage that there are constraints in the relative angle between rings, since each mirror is in common between two rings, and three linear Fabry-Pérot (FP) cavities are available using the three diagonals of the rings. Those

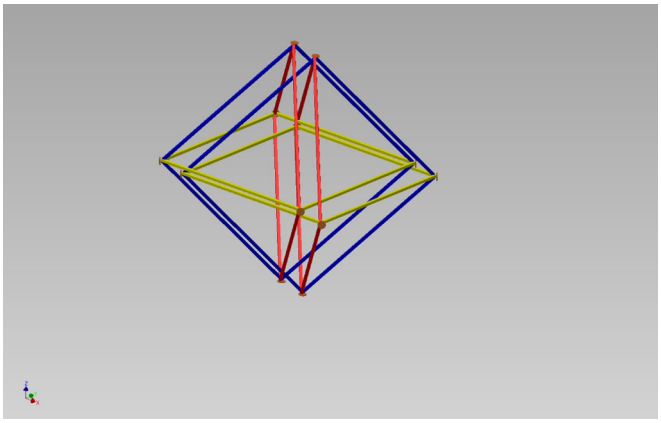

FIG. 14 (color online). Six rings, two by two parallel, with mirrors on the vertices of two octahedra, constructed very close one to the other in order to reduce the dimension of the apparatus.

linear cavities have the capability of monitoring the relative angles between different rings, and as well the length of each diagonal.

A. Ring-laser sensitivity

The rotation sensitivity σ_Ω^2 for noise fluctuations which are dominated by laser shot noise over an integration time T, reads

$$\sigma_\Omega^2 = \frac{cP}{4AQ}\sqrt{\frac{hf}{WT}}, \tag{28}$$

where Q is the quality factor of the optical cavity, $f = c/\lambda$ is the laser frequency, h is the Plank constant, and W is the power of the laser [43]. The limiting sensitivity can be conveniently calculated scaling the parameters of the Wettzell G ring laser

$$\sigma_\Omega = 2.9 \times 10^{-13}\left(\frac{P}{16\ \mathrm{m}}\right)\left(\frac{16\ \mathrm{m}^2}{A}\right)\left(\frac{3\times 10^{12}}{Q}\right) \times \left(\sqrt{\frac{20\ \mathrm{nW}}{W}}\right)\left(\sqrt{\frac{10^5\ \mathrm{s}}{T}}\right)\ \mathrm{rad/s}. \tag{29}$$

In order to obtain in few weeks a 10% accuracy level in the measurement of the relativistic effective rotation rates, we must achieve the sensitivity goal of $\sigma_\Omega = 7 \times 10^{-14}$ rad/s (or equivalently a rotation noise level 20 prad/ sec $/\mathrm{Hz}^{1/2}$ at a frequency of 1 day^{-1}). From Eq. (29) we have that a system of six rings with $P = 24$ m, $Q = 3 \times 10^{12}$, and $W = 200$ nW can fulfill this requirement.

B. Expected performances of not optimally oriented rings

We assume that the ring lasers are identical in the sense described in Sec. III E and that the dihedral angles $\arccos(\boldsymbol{u}_\alpha \cdot \boldsymbol{u}_\beta)$ are measured better than one part in 10^{10} in order to estimate Ω independently from the reference frame. Note that only the stability of dihedral angles can be monitored by means of the Earth signal itself only for short times (few days), while their measurements and controls must be performed independently in the laboratory. For instance, assuming that the scale factors are controlled to the 10^{-10} accuracy, the responses of two parallel rings are statistically different from noise when their parallelism is modified.

From an experimental point of view, to arrange in the Cartesian planes several rings and keep the configuration stable over the integration time $T \simeq 1$ day is a demanding task. However, we can relax such a demanding requirement by means of data analysis procedures that account for slightly nonorthogonal dihedral angles.

For instance, we can use the measured dihedral angles to estimate directly Ω. In fact, we can substitute the quadratic combination of ring-laser responses in Eq. (17) with the equivalent bilinear combination,

$$Q = \sum_{\alpha=1,\beta=1}^{M} Q_{\alpha\beta} R_\alpha R_\beta, \tag{30}$$

where $Q_{\alpha\beta}$ are the elements of the $M \times M$ matrix $\boldsymbol{Q} = \boldsymbol{N}(\boldsymbol{N}\boldsymbol{N}^T)^{-2}\boldsymbol{N}^T$. The statistics of Q is no longer noncentral χ^2; however, we can easily compute (see Appendix B for details) its mean

$$\langle Q \rangle = |\boldsymbol{\Omega}|^2 + M\sigma_\Omega^2 \tag{31}$$

and variance

$$\sigma_Q^2 = 2\sigma_\Omega^4 \sum_{\alpha_\beta} Q_{\alpha_\beta}^2 + 4\sigma_\Omega^2 \Omega^2 \sum_{\alpha_\beta} Q_{\alpha_\beta}^2 \boldsymbol{u}_\alpha^\parallel \boldsymbol{u}_\beta^\parallel. \tag{32}$$

In the limit of high SNR, fluctuations of Q tend to be Gaussian distributed, and so we recover the results in Eq. (22) for the overall sensitivity of the system. If we start with dihedral angle close to $\pi/2$ (say 1 part in 10^5), then sensitivity loss is very small since it is of the same order.

C. Guidelines of the experimental apparatus

The best performing ring, so far, is G which is a four mirrors ring. This is one of the reasons why the present scheme uses a square ring geometry. In principle, a triangular ring, with three mirrors could be preferable since the three mirrors are always inside a plane, and the losses will be minimized as well, reducing the number of mirrors. It could be advantageous in principle, but a triangular ring is less sensitive. For instance, let us compare the performance of two rings inscribed in a circle of radius r; for a regular polygon with different number of sides N, the area is $A = N\frac{r^2}{2}\sin(\frac{2\pi}{N})$ and the perimeter is $P = 2Nr\sin(\frac{\pi}{N})$; it is straightforward to demonstrate that the triangular ring has 0.7 times the signal than the square one, which is equivalent to say that the triangular ring needs 2 times more time to reach the same level of accuracy as the square one.

The ring-laser response is proportional to the scale factor "S." For a perfect square ring this proportionality factor is equivalent to N, the number of wavelength inside the ring: when the length of the ring changes, because of a change in the temperature, the laser changes its wavelength in order to keep N constant. This is true as long as the perimeter change is below one wavelength, 632 nm in our case, and in this condition the gain factor of the instrument guarantees a very high accuracy of the measurement. For example, if the laboratory has $\delta T = 1°$ temperature excursion, and the ring perimeter is 36 m, in order to guarantee the operation of the ring laser with a fixed number of wavelengths N, it is necessary to realize the whole apparatus using materials with temperature expansion coefficient of the order of 10^{-8} K^{-1}. This is the concept used for G in Wettzell: a structure realized with material as Zerodur, with a design which can be defined monolithic, i.e. relative motions of the mirrors are not allowed. G has a very high stability, but is rather expensive, and not very flexible with regards to changing the mirrors and aligning the laser cavity. Moreover, the extension of this design to a large array of rings seems rather difficult. Later on, a more flexible and less expensive design has been realized, called GEOSENSOR, which so far has been employed especially for smaller size rings. This design allows a very good relative alignment of the mirrors, it is relatively easy to change mirrors and tools to move each mirror along different degrees of freedom have been implemented. So far these kinds of instruments have been done in steel. Figure 15 shows a drawing of G-Pisa, our prototype. The optical cavity vacuum chamber has a stainless steel modular structure: four towers, located at the corners of the square and containing the mirrors holders inside, are connected by pipes, in order to form a ring vacuum chamber with a total volume of about 5×10^{-3} m^3. The mirrors are rigidly fixed to the tower. The cavity alignment can be adjusted by moving the towers with respect to the slab through a lever system that allows 2 degrees of freedom of movements. No window delimits the active region and the vacuum chamber is entirely filled with a mixture of He and a 50% isotopic mixture of ^{20}Ne and ^{22}Ne. The total pressure of the gas mixture is set to 560 Pa with a partial pressure of neon of 20 Pa. The active region is a plasma produced in a capillary Pyrex tube inserted at the middle of one of the ring sides, by a radio frequency capacitively coupled discharge. In a nonmonolithic device, temperature changes could interrupt the continuous operation, and the perimeter is actively controlled by acting on the mirrors and using as reference a stabilized laser; very highly stabilized lasers are commercially available, for instance wavelength stabilization at the level of 2.5×10^{11} using iodine line can be obtained. G-Pisa is kept in continuous laser operation through a perimeter stabilization servo system which acts along the diagonal direction, for two

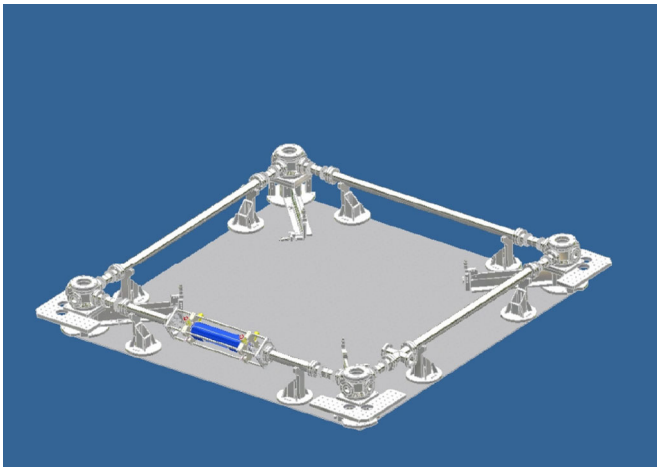

FIG. 15 (color online). Drawing of G-Pisa, based on the GEOSENSOR design.

oppositely placed mirrors, through piezoelectric actuators [44].

The GEOSENSOR design has other advantages as well: the mirrors are under vacuum and are not affected by the outside pressure changes, they can be very easily aligned and the cost is pretty much reduced compared with the monolithic design. The experience of G-Pisa has shown so far that it can work with different orientations. In fact G-Pisa has worked both horizontally and vertically oriented. It is in steel, inside the thermally stabilized room in the central area of Virgo, in order to improve thermal stability, it has been mounted on top of a granite table (thermal expansion coefficient about 5×10^{-6} m/mK). To find the guidelines of the mechanical project, we have used a simple program which consists in considering the ring as four points (the light spots on the mirrors) which can be moved from the ideal position, both inside the plane or outside the plane. The model takes into account thermal expansion and the perimeter is kept constant by acting diagonally on pairs of mirrors; the use of two mirrors or four mirrors for the feedback correction have been investigated; the thermal excursion is considered of 1 K. The scale factor S in presence of misalignments is compared with S_0 (scale factor at the optimal configuration); this comparison is expressed as $M_{\rm acc} = \frac{S_0 - S}{S_0}$, which gives the accuracy limit induced by misalignments. The required level of accuracy of 1 part of 10^{10} is $M_{\rm acc} = 10^{-10}$. Figure 16 shows $M_{\rm acc}$ for a rectangular ring, with sides 6 m and 6.6 m, in function of a misalignment of one of the four mirrors.

Figure 16 clearly shows that the gain factor changes a lot with a small change of mirror positions. The situation strongly improves by considering a perfect square ring. In fact, for a closed figure with a fixed number of sides, the area over perimeter ratio has a maximum when the polygon is a regular one, as, for example, a ''perfect'' square ring. Figures 17 and 18 show $M_{\rm acc}$ with 100 μm construction precision and two possible choices of the thermal expansion coefficient. For instance, let us assume that each mirror position is in the ideal position within a quantity δ which depends on the precision of the construction. Figure 19 shows $M_{\rm acc}$ when three out of the four mirrors are positioned with an error; 10 000 points have been evaluated pseudorandomly distributed between ± 50 μm along each coordinate. In summary, if the thermal excursion is 1 K, the position of the mirrors is an ideal square within ± 50 μm, the support has a thermal expansion coefficient below 7×10^{-7} K^{-1}, $M_{\rm acc}$ remains in the range necessary for the needed accuracy using four or two mirrors active control of the perimeter.

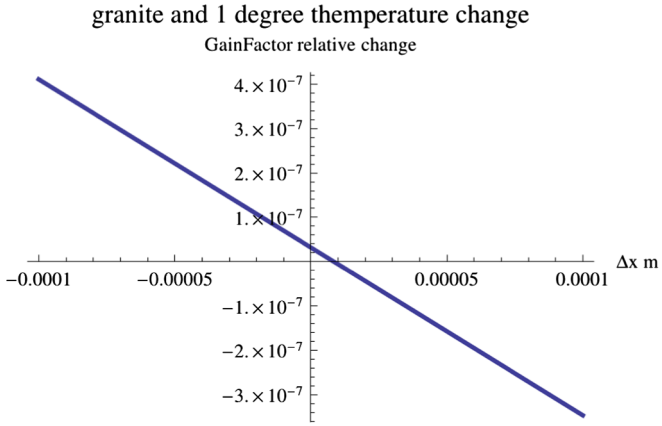

FIG. 16 (color online). $M_{\rm acc}$, for a rectangular ring, with sides 6×6.6 m, in function of a misalignment of one of the four mirrors with respect to the ideal position, the perimeter control acts on four mirrors, maximum thermal excursion of 1 K and the support of the GEOSENSOR has thermal expansion coefficient of 7×10^{-6} K^{-1} (granite).

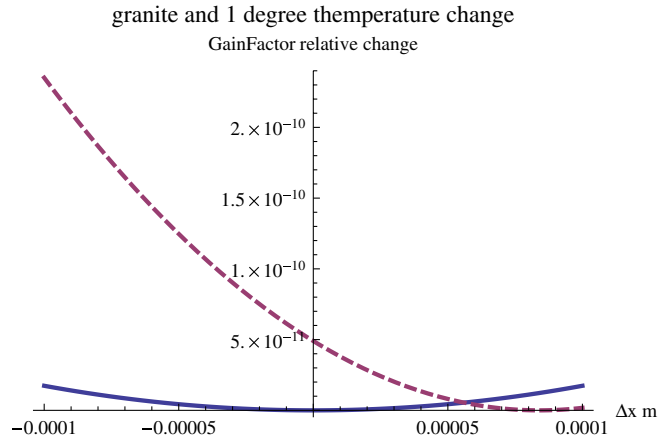

FIG. 17 (color online). $M_{\rm acc}$ in function of a misalignment of one of the four mirrors with respect to the ideal position, the perimeter control acts on four (thick line) or two (dashed line) mirrors, maximum thermal excursion of 1 Kand the material has 7×10^{-6} m/mK (granite).

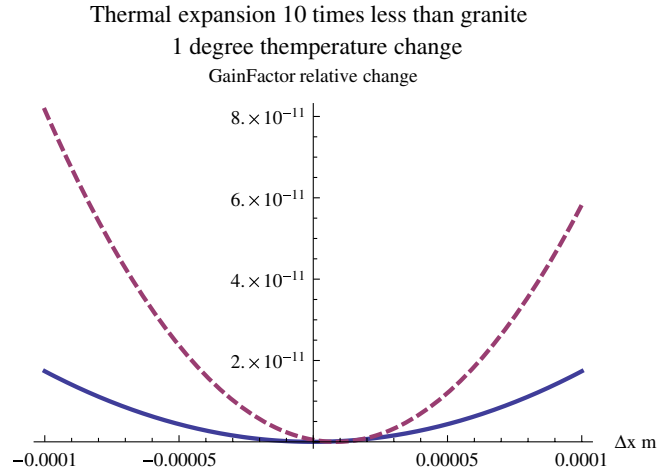

FIG. 18 (color online). Same as Fig. 17, but with expansion coefficient 10 times lower.

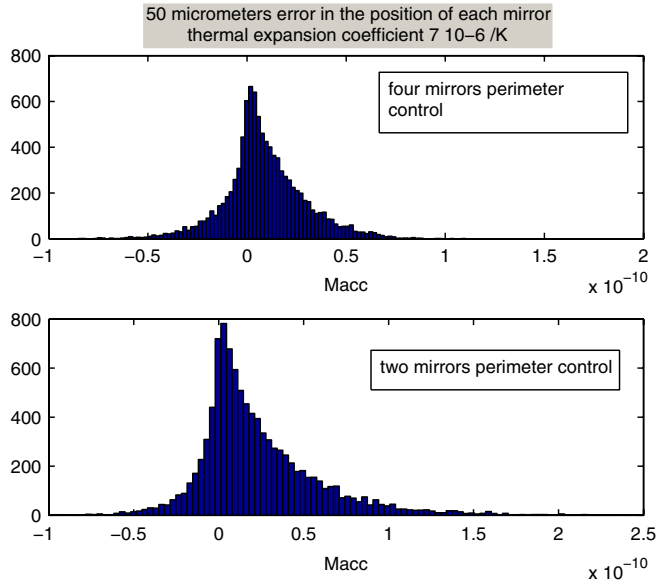

FIG. 19 (color online). Histogram of $M_{\rm acc}$ when the position of three mirrors are within ± 50 μm close to the ideal position, 10 000 points have been evaluated by randomly extracting the position error ($\pm$ 50 μm). The thermal expansion coefficient is 7×10^{-7} K^{-1}, thermal excursion 1 K, top histogram shows the case with four mirrors control of the perimeter, bottom curve with two mirrors control.

Misalignments which bring the light spots outside the plane of the ring do not have an appreciable effect on the gain factor, but they change the orientation of the area vector $\boldsymbol{u}_\alpha$; in this case the effect for $M_{\rm acc}$ depends on the relative angle between the ring and the Earth rotational axis. Figures 20 and 21 show how the accuracy changes for two different ring orientations: parallel to the axis of the

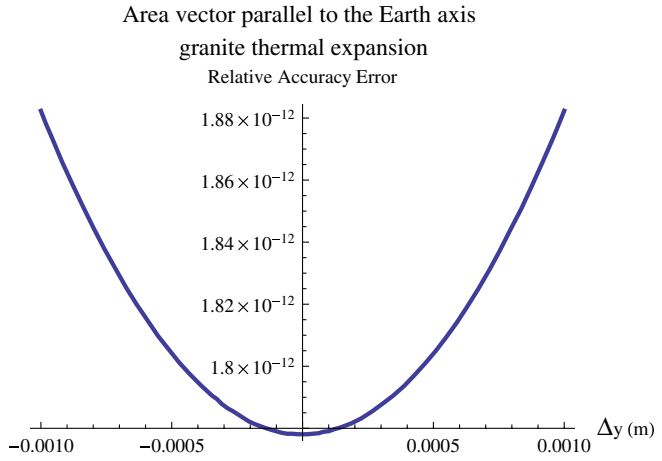

FIG. 20 (color online). Accuracy change in percentage for vertical misalignments and area vector close to the parallel alignment to the Earth rotational axis. The ring geometry is not perfect in the plane, there is a misalignment of 100 μm, a maximum temperature change of 1 K, and the thermal expansion coefficient is 7×10^{-6} m/m/K.

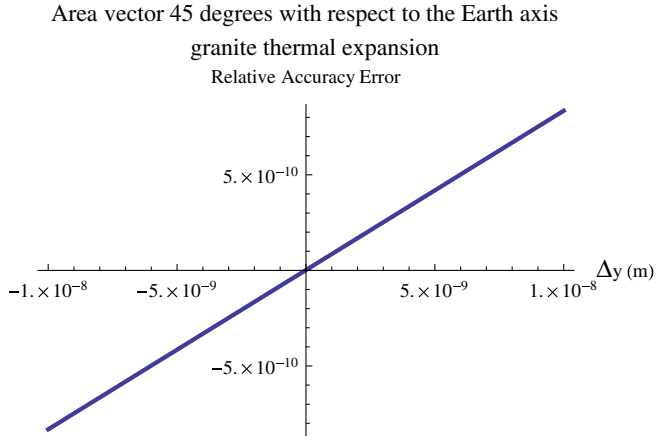

FIG. 21 (color online). Accuracy change in percentage for vertical misalignments and area vector close to 45 degrees with respect to the Earth rotational axis. The ring geometry is not perfect in the plane, there is a misalignment of 100 μm, a maximum temperature change of 1 K, and the thermal expansion coefficient is 7×10^{-6} m/m/K.

Earth and at 45° degrees, respectively. The first is almost insensitive, while the other is sensitive to nanometric misalignments.

Figure 22 shows $M_{\rm acc}$ for a nm vertical misalignment of one of the rings in function of the angle with respect to the Earth rotational axis.

In summary, the gain factor of each ring can be kept constant at the level of 1 part in 10^{10}, if the positions of the mirrors are constructed and kept within ± 50 μm error close to the ideal square ring; the relative position between mirrors can be rigidly constrained with granite, superinvar

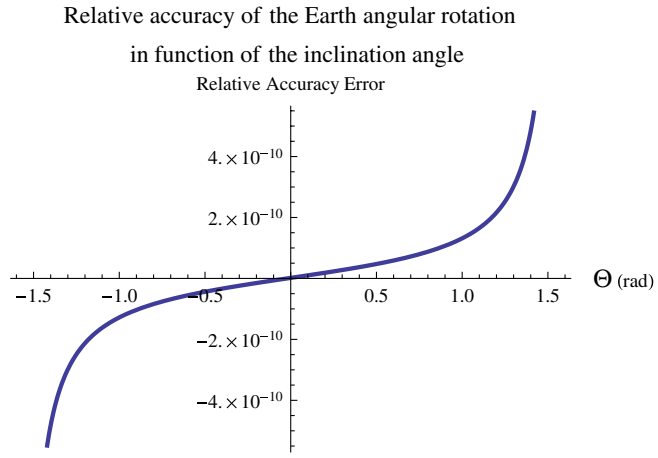

FIG. 22 (color online). Relative limit of the accuracy in the measurement of the Earth angular rotation induced by a nm change in the position of one of the mirrors with respect to its original position, in function of angle with the Earth rotation axis. The area vector of the ring lays in the meridian plane. The accuracy loss is zero when the Earth axis and the area vector are parallel, and is very high in the orthogonal alignment.

or similar low thermal expansion coefficient spacers, it is preferable to use all four mirrors for the perimeter active stabilization, but two mirrors control could be acceptable as well if the structure has thermal coefficient better than granite. It is necessary to constantly monitor the relative angle between rings with nrad precision (only the relative alignment matters). This can be accomplished looking at the modal structure of the FP cavities formed along the diagonals. Moreover, the orientation of each ring with respect to the Earth rotation axis should be such as to avoid alignment too sensitive to the relative angle (relative angle with the Earth rotation axis below 60°). Using the Earth angular velocity rotation, which is perfectly stable for a few days, the whole apparatus can be calibrated at the beginning; the relative angle, or the area of each ring could be not perfectly planar or exactly 90°, but it is important to monitor the geometry of the structure during the whole measurement time (years). The mirror holders play an important role, it can be advantageous to build them in Zerodur or similar material, in order to avoid displacements out of the plane. The mirror holders should be designed in order to provide the tools to align the cavities; in principle, each mirror should have 5 degrees of freedom: *three* translations and two tilts, the rotation around the axis orthogonal to the mirror itself does not play a role; but since the mirrors are spherical only three motions are fundamental: we may have one translation along the diagonal and two mirrors tilts or three translations.

Let us consider now an octahedral geometry, containing the three rings.

Figure 22 shows that the relative angle between the different rings must be monitored at the level of nrad, and that it should be avoided to put one of the rings with an angle larger than 60° with respect the Earth rotation axis. We have done the exercise to fit the octahedron, with rings of 24 m perimeter, inside node B of LNGS, considering that this node is 8 m tall, and imposing the constraints discussed in Fig. 22. The exercise is done with the octahedron since it needs more space. Considering that the latitude of LNGS is 42° 27″N two configurations are given: to have the octahedron straight up (8.4 m tall) or laying on one side, one ring is, respectively, horizontally or vertically oriented and the other two symmetrically positioned with respect to the meridian plane. Let us consider the maximum size 9 m: 8.48 m, the diagonal of the octahedron, plus 0.6 m necessary to hold mirrors and optics in general necessary for the readout. This octahedron can be contained inside each of the big halls of LNGS, in both orientations, but inside node B, which is the most isolated room of LNGS, see Figs. 23 and 24, the only possibility is the shorter configuration, with the longer side parallel to the floor.

So, the octahedron, with rings of 24 m perimeter, can be contained inside node B, where the ceiling is 8 m tall, while for node C the structure should be scaled, probably no

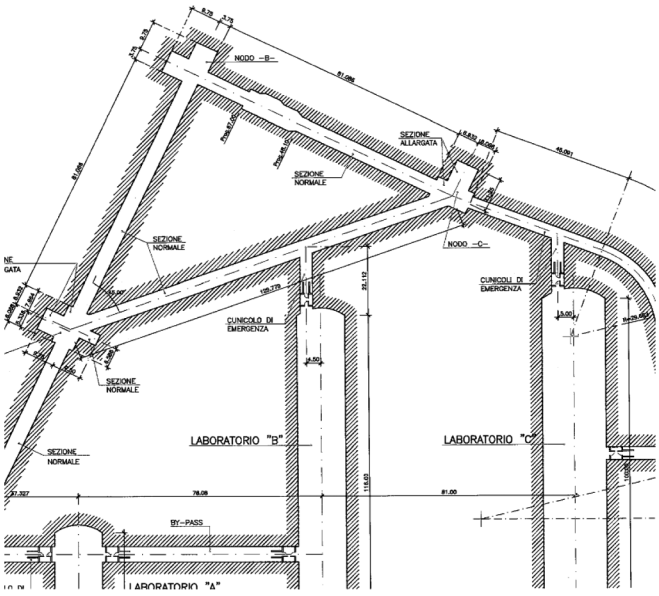

FIG. 23. Plan of LNGS laboratory close to node B.

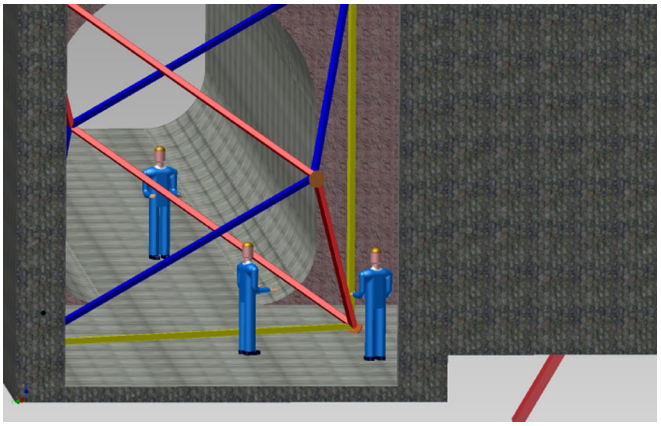

FIG. 24 (color online). The ring-laser system inside node B of LNGS, side view showing the passage between the two entrances.

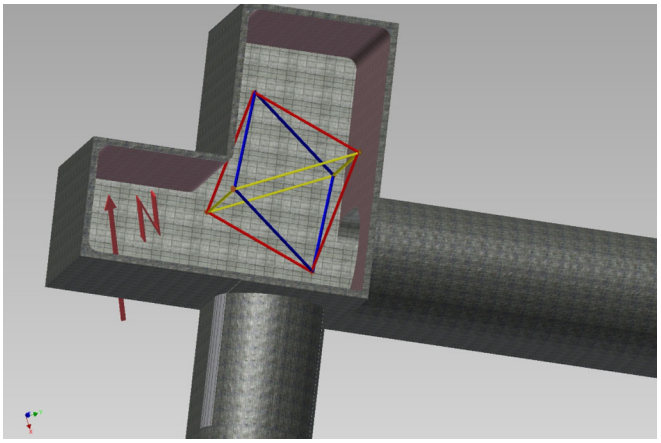

FIG. 25 (color online). The octahedron inside node B.

more than 20 m perimeter can be contained inside node C, since the ceiling there is 6 m tall. Figure 25 shows the octahedron inside node B.

VI. DIAGNOSTICS OF DIHEDRAL ANGLES AND SCALE FACTORS

To reduce the influence of systematics in long-term measurements, the control of the geometrical stability of the ring-laser system is of paramount importance. In particular, it is crucial to monitor the deviations from planarity of each ring laser and their mutual orientations.

A square ring consists of four spherical mirrors with the same curvature radius R, placed at the corners. Square geometry guarantees that opposite mirrors are parallel so that they form two extra linear Fabry-Pérot cavities (see Fig. 26). As a consequence, each square ring is made of three optical resonators: the ring itself and two linear ones oriented along the diagonals. These latter can be used to monitor the geometrical stability of the whole ring system. Deviations from a square geometry result in tilting and/or displacements of the diagonal vectors, which in turn change the cavity eigenmodes.

A linear symmetric FP cavity with spherical mirrors in $z_M = \pm\frac{1}{2}d = \pm\frac{1}{\sqrt{2}}L$ (L being the square ring arm) and centers on the z axis, supports the Gaussian modes

$$E_{\ell,m}(x,y,z) = \frac{1}{w_c(z)} H_\ell\left(\frac{\sqrt{2}x}{w_c(z)}\right) H_m\left(\frac{\sqrt{2}y}{w_c(z)}\right) \times \exp\left[-ik\frac{x^2+y^2}{2q_c(z)} - ikz + i(\ell+m+1) \times \arctan\left(\frac{2z}{b}\right)\right], \quad (33)$$

where $q_c(z) = z - ib = (\frac{1}{R_c(z)} - i\frac{\lambda}{\pi w_c^2(z)})^{-1}$ and $b = \sqrt{d(2R-d)}$ are the complex curvature of the Gaussian beam and the confocal parameter, respectively; here the curvature radius $R_c(z)$ and the spot- size $w_c(z)$ read

$$R_c(z) = \frac{d^2 - 2dR - 4z^2}{4z}$$
$$w_c^2(z) = \frac{\lambda}{\pi}\frac{4z^2 + 2dR - d^2}{2\sqrt{d(2R-d)}}.$$

The eigenmodes $E_{\ell,m}(x,y,z)$ form a complete set which can be used for representing a generic field confined between the two generally misaligned mirrors of the cavity,

$$E(x,y,z) = \sum_{\ell,m} C_{\ell,m} E_{\ell,m}(x,y,z),$$

where

$$C_{\ell m} = \int dx \int dy E_{\rm in}(x,y) E_{\ell,m}(x,y,z_M)$$

and $E_{\rm in}(x,y)$ is the beam illuminating the input mirror M_1. If we suppose the mirror tilted by Θ_x and Θ_y and displaced by X and Y with respect to cavity axis $\hat{z}$, we have

$$E_{\rm in}(x,y) \propto e^{-ik(\{(x-X)^2/[2q_c(z_M)]\}+\Theta_x x+\{(y-Y)^2/[2q_c(z_M)]\}+\Theta_y y)}.$$

As an example, the relative intensities $|C_{\ell m}|^2/|C_{00}|^2$ for the first modes $\ell + m = 0, 1, 2$ and $X = Y = 0$ are reported in Table I.

It is clear that the cavity axes misalignment can be detected by looking at the intensity pattern of the beam transmitted through the output mirror M_2. A modal decomposition of such a pattern gives a suitable set of coefficients $|C_{\ell m}|^2$ which can be used for estimating the position and angular misalignment of the cavity with respect to the reference beam $E_{\rm in}(x,y)$.

Supposing that at the beginning ($t = 0$) the cavity external laser is perfectly aligned to a symmetric cavity (if the two mirrors show equal transmittivity then the cavity transmission is 1) so that all the incoming power $P_{\rm in}$ is coupled to the TEM00 mode. The measurement procedure we have devised is a tunable laser, showing a linewidth narrower than the cavity linewidth, tuned over a cavity FSR in a time interval Δt so that each mode is spanned in a time $\tau = \frac{\Delta t}{\mathcal{F}}$, where $\mathcal{F}$ is the cavity finesse. The number of photons in the ℓm mode are given by (we are now assuming a rectangular line shape instead of a Lorentzian profile)

$$n_{\ell m} = k\frac{P_{\rm in}}{h\nu}\tau|C_{\ell m}|^2.$$

This number of photons must be higher than the noise equivalent number of photons hitting the detector in the same time interval. The noise equivalent power (NEP) in $W/\sqrt{\rm Hz}$, is connected to the equivalent number of photons by

$$n_{\rm NEP} = \frac{\rm NEP}{h\nu}\frac{\sqrt{B}}{\eta}\tau,$$

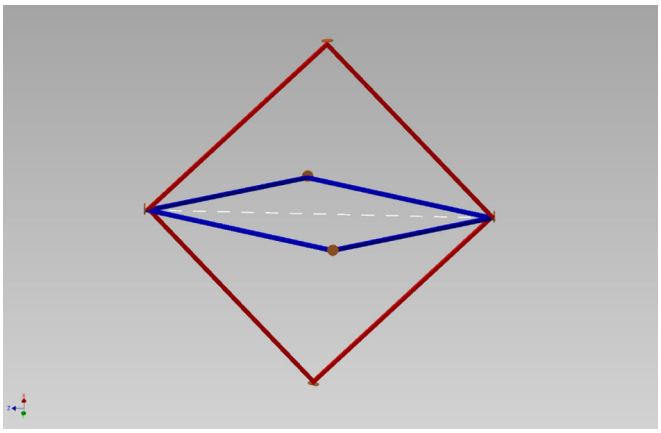

FIG. 26 (color online). In a square ring configuration passive Fabry-Pérot cavities are formed along the square diagonals (dashed line in the sketch). In the case of an octahedron each of these three passive cavities is shared by two rings.

TABLE I. Power coupled to the first cavity higher modes ($\ell + m = 0, 1, 2$) as a fraction of the external laser power for $q_c = q_x = q_y$ and $X = Y = 0$. The values are obtained for a ratio between the cavity length and the mirror radius of curvature of 1.5.

$\lvert C_{\ell m}\rvert^2/\lvert C_{00}\rvert^2$	$\ell = 0$	$\ell = 1$	$\ell = 2$
$m = 0$	1	$5.16 \times 10^7 \Theta_x^2$	$1.33 \times 10^{15} \Theta_x^4$
$m = 1$	$5.16 \times 10^7 \Theta_y^2$	$2.66 \times 10^{15} \Theta_x^2 \Theta_y^2$	
$m = 2$	$1.33 \times 10^{15} \Theta_y^4$		

where η and B are the quantum efficiency and the detection bandwidth, respectively.

To overcome the photon noise, we have to satisfy the inequality

$$\frac{n_{\mathrm{NEP}}}{n_{\ell m}} = \frac{n_{\mathrm{NEP}}}{n_{00}} \frac{|C_{00}|^2}{|C_{\ell m}|^2} < 1.$$

In particular, looking at the C_{01} coefficient we have

$$n_{00} > \frac{1}{5.16 \times 10^7 \Theta^2} \frac{\mathrm{NEP}}{h\nu} \frac{\sqrt{B}}{\eta} \tau;$$

further, by assuming $n_{00} \simeq \frac{P_{\mathrm{in}}}{h\nu} \tau$ we obtain

$$P_{\mathrm{in}} > \frac{\mathrm{NEP}\sqrt{B}}{5.16 \times 10^7 \Theta^2 \eta}.$$

For typical silicon detectors $\mathrm{NEP} \sim 10^{-14} W/\sqrt{\mathrm{Hz}}$, $B \sim 10^6$ Hz, $\eta \sim 0.9$, so that

$$P_{\mathrm{in}} > 2.2 \times 10^{-19} \Theta^{-2}.$$

For a tilt sensitivity of $\Theta \sim 10^{-9}$ the power required at the input is

$$P_{\mathrm{in}} > 220 \text{ mW}.$$

VII. MORE ABOUT THE IMPORTANCE OF THIS MEASUREMENT

A. Post-Newtonian parameters

The proposed experimental apparatus is well suited for performing an optical test of the metric theory of gravitation. We start from the statement that the vector $\boldsymbol{\Omega}'$ should be entirely contained in the meridian plane if the preferred frames effect, determined by $\boldsymbol{W}$ [see Eq. (A9)], can be neglected. Indeed the currently available best estimates [20] suggest that this effect is about 2 orders of magnitude smaller than the geodetic and Lense-Thirring contributions. As a consequence, we expect that the measured components of $\boldsymbol{\Omega}'$ outside the meridian plane should be compatible with noise. In this case, our results could be used to obtain new constraints, independent from the available ones, on the preferred frame parameters. In addition, we can write the PPN parameters α_1 and γ as a function of the $\boldsymbol{u}_r$ and $\boldsymbol{u}_\theta$ components of $\boldsymbol{\Omega}'$,

$$\begin{aligned} \alpha_1 &= (-4\hat{\Omega}'_\theta \csc\theta - 8\hat{\Omega}'_r \sec\theta] \\ \gamma - 1 &= (\hat{\Omega}'_\theta \csc\theta - \hat{\Omega}'_r \sec\theta/2) - 2, \end{aligned} \tag{34}$$

where $\hat{\Omega}'_{r,\theta} \equiv \Omega'_{r,\theta}/w$ and w is the very precisely measured constant $w \equiv 2\pi GM/(c^2 R T_S) \simeq 5.074\,779\,8 \times 10^{-14}$ rad/sec; here we have used $GM = 3.986\,004\,418 \times 10^{14}$ m^3/s^2, $R = 6.378\,137 \times 10^6$ m and $T_S = 86\,164.0989$ s. Assuming one year of data taking with the same ring-laser parameters used for the simulations in Sec. III D we have that the standard deviation of $\hat{\Omega}'_\theta$ and $\hat{\Omega}'_r$ is $\hat{\sigma}_{\Omega_{r,\theta}} \simeq 0.03$, and therefore upper limits of some interest can be put on α_1 and γ at the Gran Sasso colatitude $\theta \simeq \pi/4$.

B. Interdisciplinary: Geodesy and geophysics

The Earth rotation rate and the orientation of the rotational axis of the Earth in space are the linking quantities between the terrestrial (ITRF) and the celestial (ICRF) reference frames. Currently a set of quasars, forming an external set of markers, provide the only way of determining the rotational velocity and the variations of the orientation of the rotational axis of the Earth with sufficient accuracy. As already mentioned, 10 μs for the measurement of length of day (LoD) and 0.1 milliarcsecond (mas) for the pole position are routinely achieved by a network of VLBI radio telescopes as one of the services (IERS) of the International Association of Geodesy. The operation of such a network requires expensive equipment and a lot of maintenance effort. Huge amounts of data are recorded in each measurement session, which require physical transport over large distances for the correlation in the analysis centers. Data latency and the fact that there is no continuous measurement coverage are suggesting the investigation of alternative methods for the precise estimation of the Earth rotation. Furthermore, it is desirable to develop an independent measurement technique, in order to identify intratechnique biases if they exist. Ring lasers are possible candidates for such an alternative measurement technique. They measure the earth rotation locally and within much shorter time intervals. Such gyros are widely used in aircraft navigation and can measure rotations absolute, i.e. independent of an external reference frame. Therefore also local contributions to the Earth rotation are contained in the measurements. The effects of Earth tides, strain, crust

deformation, seismic events, and polar motion are contained in the ring-laser measurements due to their contribution to earth rotation or due to variations in the orientation of the respective ring laser. However, the demands on such instruments are extremely high and cannot be met by existing commercial devices. They can be summarized as:

(i) sensitivity to rotation 0.01 prad/s at about 1 h of integration
(ii) sensor stability of 1 part in 10^{10} over several months to years (Chandler wobble)
(iii) resolution in sensor orientation $\approx$ 1 nrad. This corresponds to polar motion of around 1 cm at the pole.

This means that a reasonable improvement in sensor sensitivity and stability is still required in order to make ring lasers viable tools to be applied to space geodesy. The design of the G ring laser is one way of approaching these demands and it is not too far away from reaching this goal [45,46]. Operating several such ring-laser gyroscopes in geophysical independent regions simultaneously offers a unique possibility to distinguish global from local (monumentation related) signal contributions through their independent data streams.

VIII. DISCUSSIONS AND CONCLUSIONS

The feasibility of the experiment for the measurement of relativistic effective rotation rates appears to rest only on a triaxial dynamical sensor of local rotation of enough sensitivity. Despite the fact that large ring lasers as G are very stable platforms and with the provision of tight feedback systems to stabilize the scale factor (cold cavity, as well as the active cavity), currently ring-laser gyroscopes are not able to determine the DC part of the Earth rotation rate with a sensitivity compatible with the requirements for detection of the Lense-Thirring effect. While the contribution of the varying Earth rotation itself presumably can be removed with sufficient accuracy from the C04 series of VLBI measurements, there remains the problem of determining the actual null-shift offsets from the laser functions in the ring-laser gyroscope. Since the gravitomagnetic effect is small and constant, a good discrimination against laser biases, such as, for example, ''Fresnel drag'' inside the laser cavity must be achieved. Therefore it will be advantageous to locally add one or several ring-laser cavities in addition to the described structures for sufficient redundancy.

Moreover, even if not strictly necessary for getting rid of all the systematics, it would be helpful to compare data taken at distant stations for having a more precise discrimination of local effects from regional and global changes. In particular, we wish to operate the G ring-laser structure in parallel to the here proposed one. Possibly a second large ring laser located at the Cashmere facility in Christchurch, New Zealand, will be useful on this respect provided that it can be run with sufficient resolution and stability.

APPENDIX A: RING-LASER MEASUREMENTS IN THE LABORATORY FRAME

In this Appendix we evaluate the response to the gravitational field of a ring laser in an Earth-bound laboratory and, to know the space-time metric in the laboratory frame we shall use the construction of the ''proper reference frame'' as described in Refs. [3,17].

As we discussed in Sec. III, a ring laser converts a time difference into a frequency difference [see e.g. Eq. (8)]. It is possible to show that (see e.g. [47]) in a stationary metric in the form [48] $g_{\mu\nu} = g_{\mu\nu}(x^i)$ an observer at rest at $x^i = x^i_0$ measures the proper-time difference $\delta\tau = \tau_+ - \tau_-$ between the right-handed beam propagation time (τ_+) and the left-handed one (τ_-):

$$\delta\tau = -2\sqrt{g_{00}(x^i_0)}\oint_{\mathcal{S}} \frac{g_{0i}}{g_{00}} ds^i = -2\sqrt{g_{00}(x^i_0)}\oint_S \boldsymbol{H}\cdot d\boldsymbol{s}, \tag{A1}$$

where $\mathcal{S}$ is the spatial trajectory of the beams, whose tangent vector is $d\mathbf{s}$, and we set $H_i = \frac{g_{0i}}{g_{00}}$.

In order to evaluate the proper-time difference (A1), we need to know the space-time metric in our laboratory, that is to say the gravitational field nearby the worldline of the observer which performs measurements with the ring laser. To this end, we consider an observer in arbitrary motion in a given background space-time, and write the corresponding local metric in a neighborhood of its worldline (see e.g. [3]):

$$g_{(0)(0)} = 1 + 2\mathcal{A}\cdot\boldsymbol{x} + O(x^2), \tag{A2}$$

$$g_{(0)(i)} = \Omega_{(i)(k)}x^{(k)} + O(x^2), \tag{A3}$$

$$g_{(i)(j)} = \eta_{(i)(j)} + O(x^2). \tag{A4}$$

It is worth pointing out that Eqs. (A2)–(A4) hold only near the worldline of the observer, where quadratic displacement terms are negligible. Here we suppose that the observer carries an orthonormal tetrad (parentheses refer to tetrad indices) $e_{(\alpha)}$, whose four-vector $e_{(0)}$ coincides with his four-velocity $\mathcal{U}$, while the four-vectors $e_{(i)}$ define the basis of the spatial vectors in the tangent space along its worldline. By construction we have $e_{(\alpha)}e_{(\beta)} = \eta_{(\alpha)(\beta)}$, where $\eta_{(\alpha)(\beta)}$ is the Minkowski tensor. The metric components (A2)–(A4) are expressed in coordinates that are associated to the given tetrad, namely, the space coordinates $x^{(i)}$ and the observer's proper time $x^{(0)}$. In the above equations, $\mathcal{A}$ is the spatial projection of the observer's 4-acceleration, while the tensor $\Omega_{(i)(k)}$ is related to the parallel transport of the basis 4-vectors along the observer's worldline: $\nabla_{\mathcal{U}}e_{(\alpha)} = -e_{(\beta)}\Omega^{(\beta)}{}_{(\alpha)}$. In particular, if $\Omega_{(i)(j)}$ were zero, the tetrad would be Fermi-Walker transported. Let us remark that the metric (A2)–(A4) is Minkowskian along the observer's worldline ($x^{(i)} = 0$); it

is everywhere flat iff $\mathcal{A} = 0$, i.e. the observer is in geodesic motion and the tetrad is nonrotating (i.e. it does not rotate with respect to an inertial-guidance gyroscope). In the latter case, the first corrections to the flat space-time metric are $O(x^2)$ [3].

In order to explicitly write the local metric, which through its gravitomagnetic (g_{0i}) and gravitoelectric (g_{00}) components enables us to evaluate the proper-time difference (A1), we must choose a suitable tetrad by taking into account the motion of the Earth-bound laboratory in the background space-time metric. To this end, we consider the following PPN background metric which describes the gravitational field of the rotating Earth (see e.g. [20]):

$$ds^2 = (1 - 2U(R))dT^2 - (1 + 2\gamma U(R))\delta_{ij}dX^i dX^j + 2\left[\frac{(1 + \gamma + \alpha_1/4)}{R^3}(\boldsymbol{J}_\oplus \wedge \boldsymbol{R})_i - \alpha_1 U(R) W_i\right]dX^i dT, \tag{A5}$$

where $-U(R)$ is the Newtonian potential, $\boldsymbol{J}_\oplus$ is the angular momentum of the Earth, W_i is the velocity of the reference frame in which the Earth is at rest with respect to mean rest-frame of the Universe; γ and α_1 are post-Newtonian parameters that measure, respectively, the effect of spatial curvature and the effect of preferred frames. The background metric (A5) is referred to an Earth-fixed inertial (ECI) frame, where Cartesian geocentric coordinates are used, such that $\boldsymbol{R}$ is the position vector and $R \doteq \sqrt{\sum_i X_i^2} = \sqrt{X^2 + Y^2 + Z^2}$. Then, we choose a laboratory tetrad which is related to the background coordinate basis of (A5) by a pure Lorentz boost, together with a renormalization of the basis vectors: in other words the local laboratory axes have the same orientations as those in the background ECI frame, and they could be physically realized by three orthonormal telescopes, always pointing toward the same distant stars.

In this case, one can show that the gravitomagnetic contribution in the local metric reads [3,17,49,50] $\Omega_{(i)(k)}x^{(k)} = -(\boldsymbol{\Omega}' \wedge \boldsymbol{x})_{(i)}$, where the total relativistic contribution $\boldsymbol{\Omega}'$ is the sum of four terms, with the dimensions of angular rotation rates

$$\boldsymbol{\Omega}' = \boldsymbol{\Omega}_G + \boldsymbol{\Omega}_B + \boldsymbol{\Omega}_W + \boldsymbol{\Omega}_T \tag{A6}$$

defined by

$$\boldsymbol{\Omega}_G = -(1 + \gamma)\boldsymbol{\nabla}U(R) \wedge \boldsymbol{V}, \tag{A7}$$

$$\boldsymbol{\Omega}_B = -\frac{1 + \gamma + \alpha_1/4}{2}\left(\frac{\boldsymbol{J}_\oplus}{R^3} - \frac{3\boldsymbol{J}_\oplus \cdot \boldsymbol{R}}{R^5}\boldsymbol{R}\right), \tag{A8}$$

$$\boldsymbol{\Omega}_W = \alpha_1 \tfrac{1}{4}\boldsymbol{\nabla}U(R) \wedge \boldsymbol{W}, \tag{A9}$$

$$\boldsymbol{\Omega}_T = -\frac{1}{2}\boldsymbol{V} \wedge \frac{d\boldsymbol{V}}{dT}. \tag{A10}$$

The vector $\boldsymbol{\Omega}'$ represents the precession rate that an inertial-guidance gyroscope, comoving with the laboratory, would have with respect to the *ideal* laboratory spatial axes (see e.g. [3,17]) which are always oriented as those of the ECI frame; if the spin vector of the gyroscope is $\boldsymbol{S}$, its precession is hence defined by

$$\frac{d\boldsymbol{S}}{dt} = \boldsymbol{\Omega}' \wedge \boldsymbol{S}. \tag{A11}$$

Differently speaking, we may say that the local spatial basis vectors are not Fermi-Walker transported along the laboratory worldline. In particular, the total precession rate is made of four contributions: (i) the geodetic or de Sitter precession $\boldsymbol{\Omega}_G$ is due to the motion of the laboratory in the curved space-time around the Earth; (ii) the Lense-Thirring precession $\boldsymbol{\Omega}_B$ is due to the angular momentum of the Earth; (iii) $\boldsymbol{\Omega}_W$ is due to the preferred frames effect; and (iv) the Thomas precession $\boldsymbol{\Omega}_T$ is related to the angular defect due to the Lorentz boost.

It is worth noticing that for a laboratory bounded to the Earth

$$\mathcal{A} \simeq \frac{d\boldsymbol{V}}{dT} - \boldsymbol{\nabla}U(R), \tag{A12}$$

and the acceleration $\mathcal{A}$ cannot be eliminated. Taking into account Eq. (A12) and substituting in Eqs. (A7) and (A10) it is possible to write the two precessions in the form

$$\boldsymbol{\Omega}_G = -(\tfrac{1}{2} + \gamma)\boldsymbol{\nabla}U(R) \wedge \boldsymbol{V}, \tag{A13}$$

and

$$\boldsymbol{\Omega}_T = \tfrac{1}{2}\mathcal{A} \wedge \boldsymbol{V}. \tag{A14}$$

In particular, for a geodetic motion (e.g. a free fall satellite) $\mathcal{A} \equiv 0$ and Eq. (A13) gives the geodetic precession for a gyroscope in free fall, while Thomas precession (A14) is zero: strictly speaking, it is just in this case that $\boldsymbol{\Omega}_G$ describes a *geodetic* effect, however the term can be also referred to the precession due to the Newtonian field of the source.

All terms in (A7)–(A10) must be evaluated along the laboratory worldline (hence, they are constant in the local frame), whose position and velocity in the background frame are $\boldsymbol{R}$ and $\boldsymbol{V}$, respectively. However, if we consider an *actual* laboratory fixed on the Earth surface, the spatial axes of the corresponding tetrad rotate with respect to the coordinate basis of the metric (A5), and we must take into account in the gravitomagnetic term (A3) the contribution of the additional rotation vector $\boldsymbol{\Omega}_\oplus$, which corresponds to the Earth rotation rate, as measured in the local frame [51].

As a consequence, it is possible to show that, up to linear displacements from the worldline, the relevant local gravitomagnetic potential turns out to be

$$g_{(0)(i)} = (\boldsymbol{\Omega} \wedge \boldsymbol{x})_{(i)}, \tag{A15}$$

where $\boldsymbol{\Omega} = -\boldsymbol{\Omega}_\oplus - \boldsymbol{\Omega}'$, while the gravitoelectric $g_{(0)(0)}$ one remains the same.

Now, we are able to evaluate the proper-time difference

$$\delta\tau = -2\sqrt{g_{00}(x_0^i)}\oint_S \boldsymbol{H}\cdot d\boldsymbol{s}. \tag{A16}$$

Without loss of generality, we suppose that the observer is at rest in the origin of the coordinates, so that, according to (A2), $g_{00}(x_0^i) = 1$. As a consequence, we have

$$\delta\tau = -2\oint_S \frac{(\boldsymbol{\Omega}\wedge\boldsymbol{x})}{(1+2\mathcal{A}\cdot\boldsymbol{x})}\cdot d\boldsymbol{s}. \tag{A17}$$

Now, on taking into account the expression of the acceleration of the laboratory frame (A12) and evaluating the magnitude of the various terms, the leading contribution to (A17) can be written, applying Stokes theorem

$$\delta\tau = -2\int_A [\boldsymbol{\nabla}\wedge(\boldsymbol{\Omega}\wedge\boldsymbol{x})]\cdot d\mathbf{A}, \tag{A18}$$

where $\mathbf{A} = A\boldsymbol{u}_n$ is the area enclosed by the beams and oriented according to its normal vector $\boldsymbol{u}_n$. On evaluating the curl, taking into account that $\boldsymbol{\Omega}$ is constant, we eventually obtain

$$\delta\tau = -4\int_A \boldsymbol{\Omega}\cdot d\mathbf{A} = -4\boldsymbol{\Omega}\cdot\mathbf{A}. \tag{A19}$$

On substituting $\boldsymbol{\Omega} = -\boldsymbol{\Omega}_\oplus - \boldsymbol{\Omega}'$ in (A19), we see that the proper-time delay can be written in the form

$$\delta\tau = 4\boldsymbol{\Omega}_\oplus\cdot\mathbf{A} + 4\boldsymbol{\Omega}'\cdot\mathbf{A}, \tag{A20}$$

where $4\boldsymbol{\Omega}_\oplus\cdot\mathbf{A}$ is the purely kinematic Sagnac term, due to the rotation of the Earth, while $4\boldsymbol{\Omega}'\cdot\mathbf{A}$ is the gravitational correction due to the contributions (A7)–(A10).

According to Sec. III A, from Eq. (A19), it is then possible to write the ring-laser equation in the form

$$\delta f = \frac{4A}{\lambda P}\mathbf{u}_n\cdot\boldsymbol{\Omega}. \tag{A21}$$

To further clarify Eqs. (A7)–(A10) it is useful to use an orthonormal spherical basis $\boldsymbol{u}_r$, $\boldsymbol{u}_\vartheta$, $\boldsymbol{u}_\varphi$ in the ECI frame, such that the $\vartheta = \pi/2$ plane coincides with the equatorial plane. As a consequence, the position vector of the laboratory with respect to the center of the Earth is $\boldsymbol{R} = R\boldsymbol{u}_r$ and the kinematic constraint $\boldsymbol{V} = \boldsymbol{\Omega}_\oplus\wedge\boldsymbol{R}$ holds, i.e. $\boldsymbol{V} = \Omega_\oplus R\sin\theta\boldsymbol{u}_\varphi$.

Thus, the components of $\boldsymbol{\Omega}'$ in physical units read

$$\boldsymbol{\Omega}_G = -(1+\gamma)\frac{GM}{c^2R}\sin\vartheta\Omega_\oplus\boldsymbol{u}_\vartheta, \tag{A22}$$

$$\boldsymbol{\Omega}_B = -\frac{1+\gamma+\alpha_1/4}{2}\frac{G}{c^2R^3}[\boldsymbol{J}_\oplus - 3(\boldsymbol{J}_\oplus\cdot\boldsymbol{u}_r)\boldsymbol{u}_r], \tag{A23}$$

$$\boldsymbol{\Omega}_W = -\frac{\alpha_1}{4}\frac{GM}{c^2R^2}\boldsymbol{u}_r\wedge\boldsymbol{W}, \tag{A24}$$

$$\boldsymbol{\Omega}_T = -\frac{1}{2c^2}\Omega_\oplus^2R^2\sin^2\vartheta\boldsymbol{\Omega}_\oplus. \tag{A25}$$

Moreover, we assume the general relativistic values of the PPN parameters, $\gamma = 1$, $\alpha_1 = 0$, and use for the Newtonian potential of the Earth its monopole approximation, i.e. $U(R) = GM/R$. Thus, the components (A22) and (A23) read

$$\boldsymbol{\Omega}_G = -2\frac{GM}{c^2R}\sin\vartheta\Omega_\oplus\boldsymbol{u}_\vartheta, \tag{A26}$$

$$\boldsymbol{\Omega}_B = -\frac{G}{c^2R^3}[\boldsymbol{J}_\oplus - 3(\boldsymbol{J}_\oplus\cdot\boldsymbol{u}_r)\boldsymbol{u}_r], \tag{A27}$$

$$\boldsymbol{\Omega}_W = 0, \tag{A28}$$

$$\boldsymbol{\Omega}_T = -\frac{1}{2c^2}\Omega_\oplus^2R^2\sin^2\vartheta\boldsymbol{\Omega}_\oplus, \tag{A29}$$

and, to leading order, the total rotation rate which enters Eq. (A20) is

$$\boldsymbol{\Omega} = -\boldsymbol{\Omega}_\oplus + 2\frac{GM}{c^2R}\sin\vartheta\Omega_\oplus\boldsymbol{u}_\theta + \frac{G}{c^2R^3}[\boldsymbol{J}_\oplus - 3(\boldsymbol{J}_\oplus\cdot\boldsymbol{u}_r)\boldsymbol{u}_r]. \tag{A30}$$

If we denote by α the angle between the radial direction $\boldsymbol{u}_r$ and the normal vector $\boldsymbol{u}_n$, on setting $\boldsymbol{u}_n = \cos\alpha\boldsymbol{u}_r + \sin\alpha\boldsymbol{u}_\theta$ in (A20), and using (A30), we may express the proper-time delay in the form

$$\delta\tau = \frac{4A}{c^2}\Big[\Omega_\oplus\cos(\theta+\alpha) - 2\frac{GM}{c^2R}\Omega_\oplus\sin\theta\sin\alpha + \frac{GI_\oplus}{c^2R^3}\Omega_\oplus(2\cos\theta\cos\alpha + \sin\theta\sin\alpha)\Big], \tag{A31}$$

where we have written $\boldsymbol{J}_\oplus = I_\oplus\boldsymbol{\Omega}_\oplus$, in terms of the $I_\oplus$, the moment of inertia of the Earth.

APPENDIX B: PROBABILITY DISTRIBUTION OF QUADRATIC FORMS

The statistics of quadratic forms of Gaussian random vectors $\boldsymbol{x}$ are well known in the literature. In particular, if $\boldsymbol{x}$ is a multivariate Gaussian random vector with mean $\boldsymbol{s}$ and covariance matrix $\boldsymbol{\Sigma}$, the mean and the variance of a quadratic form $Q = \boldsymbol{x}^T\boldsymbol{Q}\boldsymbol{x}$ are given by

$$\langle Q\rangle \equiv \langle\boldsymbol{x}^T\boldsymbol{Q}\boldsymbol{x}\rangle = \mathrm{Tr}(\mathbf{Q}\boldsymbol{\Sigma}) + \boldsymbol{s}^T\boldsymbol{Q}\boldsymbol{s}$$
$$\sigma_Q^2 \equiv \langle(\boldsymbol{x}^T\boldsymbol{Q}\boldsymbol{x})^2\rangle - \langle Q\rangle^2 = 2\,\mathrm{Tr}(\boldsymbol{Q}\boldsymbol{\Sigma}\boldsymbol{Q}\boldsymbol{\Sigma}) + 4\boldsymbol{s}^T\boldsymbol{Q}\boldsymbol{\Sigma}\boldsymbol{Q}\boldsymbol{s}, \tag{B1}$$

where $\boldsymbol{Q}$ is a square symmetric matrix, T and Tr are the transpose and trace operators, respectively. The statistics of Q in general is not known, unless $\boldsymbol{Q}\boldsymbol{\Sigma}$ is an idempotent matrix [52]. In the case were $\boldsymbol{x}$ represents the response of

ring lasers in a regular polyhedral configuration $\boldsymbol{Q} = \boldsymbol{I}$, with no common noise source and the same sensitivity $\boldsymbol{\Sigma} = \sigma^2 \boldsymbol{I}$, where $\boldsymbol{I}$ is the identity matrix, the above formulas greatly simplify

$$\langle Q \rangle = M\sigma^2 + E \tag{B2}$$

$$\sigma_Q^2 = 2M\sigma^4 + 4E\sigma^2, \tag{B3}$$

where $E = \boldsymbol{s}^t\boldsymbol{s} = \|\boldsymbol{s}\|^2$ is the signal energy. In this case also the statistics of Q readily follows. In fact, starting from its definition we have

$$P_Q(Q) \equiv \int P(\boldsymbol{x})\delta(Q - \boldsymbol{x}^T\boldsymbol{x})d\boldsymbol{x}, \tag{B4}$$

where $P(\boldsymbol{x}) = \exp[(\boldsymbol{x} - \boldsymbol{s})^T(\boldsymbol{x} - \boldsymbol{s})/(2\sigma^2)]/(2\pi\sigma^2)^{M/2}$ is the Gaussian probability density of one sample of the random vector $\boldsymbol{x}$. We can use the integral representation of the Dirac's δ function

$$\delta(Q - \boldsymbol{x}^T\boldsymbol{x}) = \int_{-\infty}^{+\infty} e^{i\omega(Q - \boldsymbol{x}^T\boldsymbol{x})}d\omega \tag{B5}$$

and write

$$P_Q(Q) = \int_{-\infty}^{+\infty} d\omega e^{i\omega Q} \frac{1}{(2\pi\sigma^2)^{M/2}} \times \int \exp\left[i\omega \boldsymbol{x}^T\boldsymbol{x} - \frac{1}{2\sigma^2}(\boldsymbol{x} - \boldsymbol{s})^T(\boldsymbol{x} - \boldsymbol{s})\right] d\boldsymbol{x}.$$

By rearranging the exponent, the last integral can be recast as a M-dimensional Gaussian integral and calculated explicitly,

$$\frac{1}{(2\pi\sigma^2)^{M/2}} \int \exp\left[\left(i\omega - \frac{1}{2\sigma^2}\right)\boldsymbol{x}^T\boldsymbol{x} + \frac{1}{\sigma^2}\boldsymbol{s}^T\boldsymbol{x} - \frac{E}{\sigma^2}\right] d\boldsymbol{x} = \frac{\exp[i\omega\sigma^2 E/(1 - 2i\omega\sigma^2)]}{(1 - 2i\omega\sigma^2)^{M/2}}, \tag{B6}$$

where in the last expression one recognizes the moment generating functions of noncentral χ^2 distributions with M degrees of freedom and noncentrality parameter E. The probability density function of Q can be found using the tables of Fourier transform pairs,

$$P_Q(Q) = \int_{-\infty}^{+\infty} d\omega e^{i\omega Q}\left\{\frac{\exp[i\omega\sigma^2 E/(1 - 2i\omega\sigma^2)]}{(1 - 2i\omega\sigma^2)^{M/2}}\right\} = \frac{1}{2}\exp[-(Q + E)/(2\sigma^2)] \times \left(\frac{Q}{E}\right)^{((M-2)/(4))} I_{M/2-1}(\sqrt{QE}/\sigma^2)),$$

where $I_k(x)$ are the modified Bessel functions of order k.

APPENDIX C: PROBABILITY DISTRIBUTION OF PROJECTORS

The norm of complementary projection operators $\boldsymbol{P}$ and $\boldsymbol{Q}$ acting on Gaussian random vectors $\boldsymbol{x}$ are described by remarkably simple statistics. In fact, starting from the definition of $E_P = \|\boldsymbol{P}\boldsymbol{x}\|^2$ and $E_Q = \|\boldsymbol{Q}\boldsymbol{x}\|^2$ we have that the joint probability density $P(E_P, E_Q)$ reads

$$P(E_P, E_Q) = \int P(\boldsymbol{x})\delta(E_P - \boldsymbol{x}^T\boldsymbol{P}\boldsymbol{x})\delta(E_Q - \boldsymbol{x}^T\boldsymbol{Q}\boldsymbol{x})d\boldsymbol{x}, \tag{C1}$$

where $P(\boldsymbol{x})$ is the probability density of one sample of the random vector $\boldsymbol{x}$. The two Dirac δ functions can be written using their Fourier transforms,

$$P(E_P, E_Q) = \int P(\boldsymbol{x})e^{[uE_P + vE_Q - \boldsymbol{x}^T(u\boldsymbol{P} + v\boldsymbol{Q})\boldsymbol{x}]}dudvd\boldsymbol{x}, \tag{C2}$$

where the integrals in du and dv are performed along the imaginary axis (i.e. $u = i\omega_1$ and $v = i\omega_2$ are purely imaginary complex numbers). Now assume the noise is Gaussian distributed, uncorrelated between different detectors, and with identical variance σ^2 in every detector, namely,

$$P(\boldsymbol{x}) = \frac{1}{(2\pi\sigma^2)^{(M/2)}}\exp\left(-\frac{1}{2\sigma^2}(\boldsymbol{x} - \boldsymbol{s})^T(\boldsymbol{x} - \boldsymbol{s})\right), \tag{C3}$$

where $\boldsymbol{s} \equiv (\boldsymbol{\Omega}\cdot\boldsymbol{u}_1, \ldots \boldsymbol{\Omega}\cdot\boldsymbol{u}_M)$ is the rotation signal in vectorial form. Then

$$P(E_P, E_Q) = \left(\frac{\alpha}{\pi}\right)^{(M/2)} \int \exp[-\alpha(\boldsymbol{x} - \boldsymbol{s})^T(\boldsymbol{x} - \boldsymbol{s})] \times \exp[-\boldsymbol{x}^T(u\boldsymbol{P} + v\boldsymbol{Q})\boldsymbol{x}]d\boldsymbol{x}\cdot e^{uE_P}e^{vE_Q}dudv, \tag{C4}$$

where $\alpha = 1/2\sigma_\Omega^2$. Writing $\boldsymbol{x}$ as $\boldsymbol{s} + \boldsymbol{\varepsilon}$ and switching the integration variable to $\boldsymbol{\varepsilon}$ yields

$$P(E_P, E_Q) = \left(\frac{\alpha}{\pi}\right)^{(M/2)} \int \exp[-\boldsymbol{n}^T(\alpha\boldsymbol{I} + u\boldsymbol{P} + v\boldsymbol{Q})\boldsymbol{n} - 2\boldsymbol{n}^T(u\boldsymbol{P} + v\boldsymbol{Q})\boldsymbol{s}]d\boldsymbol{\varepsilon} \times \exp[-\boldsymbol{s}^T(u\boldsymbol{P} + v\boldsymbol{Q})\boldsymbol{s}]e^{uE_P}e^{vE_Q}dudv. \tag{C5}$$

The integration in $d\boldsymbol{n}$ can be done by noting that it is a standard M-dimensional Gaussian integral with the linear term, and in general, for any $M \times M$ symmetric matrix $\boldsymbol{A}$ and M-vector $\boldsymbol{b}$,

$$\int \exp\left(-\boldsymbol{n}^T\boldsymbol{A}\boldsymbol{n} + \boldsymbol{b}^T\boldsymbol{n}\right)d\boldsymbol{n} = \frac{\pi^{M/2}}{\sqrt{\det(\boldsymbol{A})}}\exp\left(\frac{\boldsymbol{b}^T\boldsymbol{A}^{-1}\boldsymbol{b}}{4}\right). \tag{C6}$$

In our case,

$$\boldsymbol{A} = \alpha\boldsymbol{I} + u\boldsymbol{P} + v\boldsymbol{Q} \qquad \boldsymbol{b} = 2(u\boldsymbol{P} + v\boldsymbol{Q})\boldsymbol{s}. \tag{C7}$$

Now we exploit the properties of $\boldsymbol{P}$ and $\boldsymbol{Q}$. Using their complementarity, we can write

$$\boldsymbol{A} = (\alpha + u)\boldsymbol{P} + (\alpha + v)\boldsymbol{Q} \tag{C8}$$

and from the fact that they are orthogonal and idempotent we also have

$$\boldsymbol{A}^{-1} = (\alpha + u)^{-1}\boldsymbol{P} + (\alpha + v)^{-1}\boldsymbol{Q}, \tag{C9}$$

hence,

$$\boldsymbol{b}^T\boldsymbol{A}^{-1}\boldsymbol{b} = 4\left(\frac{u^2}{\alpha + u}\boldsymbol{s}^T\boldsymbol{P}\boldsymbol{s} + \frac{v^2}{\alpha + v}\boldsymbol{s}^T\boldsymbol{Q}\boldsymbol{s}\right). \tag{C10}$$

Furthermore, as $\boldsymbol{P}$ and $\boldsymbol{Q}$ are projection matrices, their eigenvalues are $\{0, 1\}$ with multiplicities, respectively, $\{M - 2, 2\}$ for $\boldsymbol{P}$ and $\{2, M - 2\}$ for $\boldsymbol{Q}$. Then, writing $\boldsymbol{A}$ in diagonal form is trivial and leads to

$$\det(\boldsymbol{A}) = (\alpha + u)^2(\alpha + v)^{M-2}, \tag{C11}$$

determinants being independent from the basis. By using (C10) and (C11) in (C6), one can see that the Gaussian integral splits into the product of factors involving either u or v. By further substituting in (C6), the remaining integrals separate and the probability density remarkably factorizes as

$$P(E_P, E_Q) = P(E_P)P(E_Q) \tag{C12}$$

with

$$P(E_P) = \int \frac{1}{1 + 2\sigma^2 u}\exp\left(\frac{-s_p u}{1 + 2\sigma^2 u}\right)e^{uE_P}du$$
$$P(E_Q) = \int\left(\frac{1}{1 + 2\sigma^2 v}\right)^{((M)/(2))-1}\exp\left(\frac{-s_q v}{1 + 2\sigma^2 v}\right)e^{vE_Q}dv \tag{C13}$$

and $s_p = \boldsymbol{s}^T\boldsymbol{P}\boldsymbol{s}$, $s_q = \boldsymbol{s}^T\boldsymbol{Q}\boldsymbol{s}$. The transformed functions are the moment generating functions of two noncentral χ^2 distributions, with 2 and $M - 2$ degrees of freedom, respectively, and whose noncentrality parameters are $\boldsymbol{s}^T\boldsymbol{P}\boldsymbol{s}$ and $\boldsymbol{s}^T\boldsymbol{Q}\boldsymbol{s}$, respectively. Thus,

$$P(E_P) = \frac{1}{2}\exp\left(-\frac{E_P + s_p}{2\sigma^2}\right)I_0\left(\frac{\sqrt{E_P s_p}}{\sigma^2}\right)$$
$$P(E_Q) = \frac{1}{2}\exp\left(-\frac{E_Q + s_q}{2\sigma^2}\right)\left(\frac{E_Q}{s_q}\right)^{((M)/(4))-1} \times I_{((M)/(2))-2}\left(\frac{\sqrt{E_Q s_q}}{\sigma^2}\right), \tag{C14}$$

where $I_n(x)$ is the modified Bessel function of the first kind. Some interesting conclusions can be drawn about the virtual channels E_P and E_Q, which make them interesting for the identification of meridian plane and the estimate of $\boldsymbol{\Omega}$.

(1) E_P is distributed as a noncentral χ^2 with 2 degrees of freedom and noncentrality parameter equal to $\boldsymbol{s}^T\boldsymbol{P}\boldsymbol{s}$, i.e. the magnitude of the signal projection in the P subspace.
(2) E_Q is distributed as a noncentral χ^2 with $M - 2$ degrees of freedom and noncentrality parameter equal to $\boldsymbol{s}^T\boldsymbol{Q}\boldsymbol{s}$, i.e. the magnitude of the signal projection in the $\mathcal{Q}$ subspace.
(3) E_P and E_Q are *statistically independent* processes.
(4) In the limit of high SNR, E_P and E_Q are Gaussian distributed with means $\langle E_P\rangle = \boldsymbol{s}^T\boldsymbol{P}\boldsymbol{s}$, $\langle E_Q\rangle = \boldsymbol{s}^T\boldsymbol{Q}\boldsymbol{s}$ and variances $\sigma^2_{E_P} = 4\sigma^2_{\Omega}\boldsymbol{s}^T\boldsymbol{P}\boldsymbol{s}$, $\sigma^2_{E_Q} = (M-2)\sigma^2_{\Omega}\boldsymbol{s}^T\boldsymbol{Q}\boldsymbol{s}$, respectively.

[1] I. I. Shapiro *et al.*, Phys. Rev. Lett. **26**, 1132 (1971).
[2] N. Straumann, *General Relativity and Relativistic Astrophysics* (Springer-Verlag, Berlin, 1991).
[3] C. W. Misner, K. S. Thorne, and J. A. Wheeler, *Gravitation* (Freeman, San Francisco, 1973).
[4] H. Thirring, Phys. Z. **19**, 204 (1918).
[5] I. Ciufolini and E. Pavlis, Nature (London) **431**, 958 (2004); I. Ciufolini *et al.*, Space Sci. Rev. **148**, 71 (2009).
[6] C. W. F. Everitt *et al.*, Phys. Rev. Lett. **106**, 221101 (2011).
[7] L. Iorio, D. M. Lucchesi, and I. Ciufolini, Classical Quantum Gravity **19**, 4311 (2002).
[8] G. E. Stedman, K. U. Schreiber, and H. R. Bilger, Classical Quantum Gravity **20**, 2527 (2003).
[9] M. O. Scully, M. S. Zubairy, and M. P. Haugan, Phys. Rev. A **24**, 2009 (1981).
[10] A. Di Virgilio *et al.*, Int. J. Mod. Phys. D **19**, 2331 (2010).
[11] F. Hasselbach and M. Nicklaus, Phys. Rev. A **48**, 143 (1993).
[12] S. A. Werner, J. L. Staudenmann, and R. Colella, Phys. Rev. Lett. **42**, 1103 (1979).
[13] J. E. Zimmermann and J. E. Mercereau, Phys. Rev. Lett. **14**, 887 (1965).
[14] F. Riehle, Th. Kirsters, A. Witte, J. Helmcke, and Ch. J. Bordé, Phys. Rev. Lett. **67**, 177 (1991).
[15] R. W. Simmonds *et al.*, Nature (London) **412**, 55 (2001).
[16] E. Hoskinsons *et al.*, Phys. Rev. B **74**, 100509(R) (2006).
[17] I. Ciufolini and J. A. Wheeler, *Gravitation and Inertia* (Princeton University Press, Princeton, 1995).
[18] L. I. Schiff, Proc. Natl. Acad. Sci. U.S.A. **46**, 871 (1960).
[19] D. Raine and E. Thomas, *Black Holes—An Introduction* (World Scientific, Singapore, 2009).
[20] C. M. Will, Living Rev. Relativity **9**, 3 (2006), http://www.livingreviews.org/lrr-2006-3.

[21] I. Ciufolini, Classical Quantum Gravity **17**, 2369 (2000).

[22] M. Bourgay *et al.*, Nature (London) **426**, 531 (2003).

[23] A. Tartaglia, Classical Quantum Gravity **17**, 2381 (2000).

[24] A. Tartaglia, A. Nagar, and M. L. Ruggiero, Phys. Rev. D **71**, 023003 (2005).

[25] J. F. Bell, F. Camilo, and T. Damour, Astrophys. J. **464**, 857 (1996).

[26] T. Damour and D. Vokrouhlický, Phys. Rev. D **53**, 6740 (1996).

[27] G. E. Stedman, Rep. Prog. Phys. **60**, 615 (1997).

[28] Time series of the daily estimate of Earth rotation vector can be downloaded from http://www.iers.org/IERS/EN/DataProducts/EarthOrientationData/eop.html and http://data.iers.org/products/176/11165/orig/eopc04_05.62-now.

[29] See, e.g., http://www.med.ira.inaf.it/index_EN.htm.

[30] See, e.g., http://www.asi.it/en/flash_en/observing/space_geodesy_center

[31] E. Mantovani, D. Albarello, C. Tarnburelli, and M. Viti, Ann. Geophys. **38**, 67 (1995); R. Haas, E. Gueguen, H. Scherneck, A. Nothnagel, and J. Campbell, Earth Planets Space **52**, 759 (2000).

[32] K. U. Schreiber *et al.*, J. Geophys. Res. **109**, B06405 (2004).

[33] K. U. Schreiber, A. Velikoseltsev,M. Rothacher, T. Klügel, G. E. Stedman, and D. L. Wiltshire, J. Geophys. Res. **109**, B06405 (2004).

[34] A. Brzezinski, Manusc. Geod. **11**, 226 (1986).

[35] G. Jentzsch, M. Liebing, and A. Weise, Bulletin Inf. Marees Terrestres **115**, 8498 (1993).

[36] H.-J. Kumpel, Habilitationsschrift, University of Kiel, 1989, p. 198.

[37] A. Weise, G. Jentzsch, A. Kiviniemi, and J. Kaariainen, J. Geodyn. **27**, 237 (1998).

[38] T. Jahr, G. Jentzsch, and A. Weise, Geodynamics **48**, 126 (2009).

[39] J. C. Harrison, J. Geophys. Res. **81/2**, 319 (1976).

[40] J. C. Harrison and K. Herbst, Geophys. Res. Lett. **4/11**, 535 (1976).

[41] A. Gebauer, C. Kroner, and T. Jahr, Geophys. J. Int. **177**, 586 (2009).

[42] A. Gebauer, H. Steffen, C. Kroner, and T. Jahr, Geophys. J. Int. **181**, 1593 (2010).

[43] K. U. Schreiber, J-P. R. Wells, and G. E. Stedman, Gen. Relativ. Gravit. **40**, 935 (2008).

[44] J. Belfi, N. Beverini, F. Bosi, G. Carelli, A. Di Virgilio, E. Maccioni, A. Ortolan, and Fabio Stefani, Appl. Phys. B (2011).

[45] K. U. Schreiber, T. Klugel, A. Velikoseltsev, W. Schlater, G. E. Stedman, and J-P. Wells, Pure Appl. Geophys. **166**, 1485 (2009); **166**, 498 (2009).

[46] K. U. Schreiber, T. Klügel, J.-P. R. Wells, R. B. Hurst, and A. Gebauer, Phys. Rev. Lett. **107**, 173904 (2011).

[47] E. Kajari, M. Buser, C. Feiler, and W. P. Schleich, Riv. Nuovo Cimento Soc. Ital. Fis. **32**, 339 (2009).

[48] Greek and Latin indices denote space-time and spatial components, respectively; letters in boldface indicate spatial vectors, while letters in italic indicate four-vectors and four-tensors; summation and differentiation conventions are assumed. In this Appendix, if not otherwise stated, we use units such that $G = c = 1$.

[49] M. C. Angonin-Willaime, X. Ovido, and Ph. Tourrenc, Classical Quantum Gravity **36**, 411 (2004).

[50] N. Ashby and B. Shahid-Saless, Phys. Rev. D **42**, 1118 (1990).

[51] For an Earth-bound laboratory, it is $\mathbf{\Omega}_\oplus \simeq [1 + U(R) + \frac{1}{2}\Omega_0^2 R^2 \sin^2\vartheta]\mathbf{\Omega}_0$, where R is the terrestrial radius, ϑ is the colatitude angle of the laboratory, and $\mathbf{\Omega}_0$ is the terrestrial rotation rate, as measured in an asymptotically flat inertial frame.

[52] A. M. Mathai and S. B. Provost, *Quadratic Forms in Random Variables: Theory and Applications* (Marcel Dekker, New York, 1992).